

University of Alberta

# **The Influence of Geometry on the Performance of Catalytic Converter**

By

**Amirhassan Najafi Marghmaleki**

A thesis submitted to the Faculty of Graduate Studies and Research in partial fulfilment of the requirements for the degree of

**Master of Science**

in

**Chemical Engineering**

**Department of Chemical and Materials Engineering**

**©Amirhassan Najafi Marghmaleki**

**Fall 2010**

**Edmonton, Alberta**

Permission is hereby granted to the University of Alberta Libraries to reproduce single copies of this thesis and to lend or sell such copies for private, scholarly or scientific research purposes only. Where the thesis is converted to, or otherwise made available in digital form, the University of Alberta will advise potential users of the thesis of these terms.

The author reserves all other publication and other rights in association with the copyright in the thesis and, except as herein before provided, neither the thesis nor any substantial portion thereof may be printed or otherwise reproduced in any material form whatsoever without the author's prior written permission

## **Examining Committee**

Robert E. Hayes, Chemical and Materials Engineering

Anthony Yeung, Chemical and Materials Engineering

Jason Olfert, Mechanical Engineering

## **Dedication**

I would like to dedicate this work to my dearest parents whom their unconditional love and support has been the most precious thing in my life. I also dedicate this work to my wonderful friends for their invaluable support and patience.

# Abstract

In this thesis, the development and use of a transient heterogeneous 2D model for monolithic catalytic converter is presented. Study on the cold flow hydrodynamics, temperature effect and CO conversion and light off behaviour of different models is developed. Different models are studied based on different parameters such as monolith brick CPSI configuration, size of the converter, inlet cone sizing and inlet velocity of the converter. The results for both steady state and transient modes are presented in detail.

It is shown that monolith brick CPSI has a significant effect on pressure drop and light-off behaviour of the converter. Also, converter size has a major effect on the performance of a converter. Inlet cone sizing showed to have a significant effect on the hydrodynamics of the converter but it did not have a major effect on light-off behaviour of the converter.

# Acknowledgment

I would like to acknowledge the people, without whom, this work would not have been possible.

- My M.Sc. supervisor, Dr. Robert E. Hayes, who gave me an exceptional opportunity to learn in my pursuit to be a good researcher. Through his knowledge, understanding and invaluable support, he guided me and taught me how to research and explore in my academic path. I am really grateful for his patience, wisdom and wonderful personality.
- Dr. Joe Mmbaga, whom without his help and support, this work could not be done. I would like to thank him for his time, kindness, guidance and wonderful advices through my work. I really enjoyed working with him.
- Last but not the least, I am honoured to have a lovely family and many dear friends and I am thankful to them for being by my side during this time. I always will be thankful for their love, encouragement and support.

# Table of Contents

<b>Chapter 1: Introduction.....</b>	<b>1</b>
<b>Chapter 2 : Background .....</b>	<b>3</b>
<b>2.1 Greenhouse gas concerns and global warming.....</b>	<b>3</b>
<b>2.2 Catalytic converter .....</b>	<b>4</b>
<b>2.2.1 Monolith converters.....</b>	<b>7</b>
<b>2.3 Modeling of monolith converters .....</b>	<b>9</b>
<b>Chapter 3: Model development and methodology .....</b>	<b>15</b>
<b>3.1 Model characteristics .....</b>	<b>15</b>
<b>3.1.1 Geometry.....</b>	<b>15</b>
<b>3.1.2 Monolith properties .....</b>	<b>16</b>
<b>3.1.3 Feed properties .....</b>	<b>17</b>
<b>3.2 Mathematical model for kinetics with internal and external mass transfer ....</b>	<b>18</b>
<b>3.2.1 Kinetic equation.....</b>	<b>19</b>
<b>3.2.2 Internal mass transfer .....</b>	<b>19</b>
<b>3.2.3 External mass transfer.....</b>	<b>20</b>
<b>3.2.4 Parameter values for the study.....</b>	<b>22</b>
<b>3.3 The conservation equations.....</b>	<b>23</b>
<b>3.3.1 Momentum balances.....</b>	<b>23</b>
<b>3.3.2 Mole balance fluid.....</b>	<b>26</b>
<b>3.3.3 Energy balances .....</b>	<b>27</b>
<b>3.4 Implementing the model in FLUENT .....</b>	<b>28</b>
<b>3.4.1 Source terms .....</b>	<b>29</b>
<b>3.4.2 Boundary Conditions.....</b>	<b>29</b>

<b>Chapter 4 : Simulation results and discussion .....</b>	<b>32</b>
<b>4.1 Cold flow results .....</b>	<b>32</b>
<b>4.1.1 Pressure profiles in the monolith.....</b>	<b>33</b>
<b>4.1.2 Velocity profiles in the monolith .....</b>	<b>39</b>
<b>4.1.3 Turbulent kinetic energy profiles in the monolith .....</b>	<b>41</b>
<b>4.1.4 Effect of inlet cone length on hydrodynamics of the converter .....</b>	<b>45</b>
<b>4.2 Temperature effect in catalytic converter, heterogeneous model .....</b>	<b>49</b>
<b>4.2.1 The effect of CPSI:.....</b>	<b>49</b>
<b>4.2.2 The effect of size on temperature profile: .....</b>	<b>54</b>
<b>4.3 Conversion profiles in the converter .....</b>	<b>56</b>
<b>4.3.1 The effect of CPSI on conversion profile.....</b>	<b>57</b>
<b>4.3.2 The effect of converter size on conversion profiles .....</b>	<b>58</b>
<b>4.3.3 The effect of inlet cone on conversion profiles .....</b>	<b>59</b>
<b>Chapter 5 : Conclusion and recommendations .....</b>	<b>61</b>
<b>5.1 Conclusions.....</b>	<b>61</b>
<b>5.2 Recommendations .....</b>	<b>62</b>
<b>References .....</b>	<b>64</b>

## List of Tables

Table 3.1- Sizing specification of the modeled converters.....	16
Table 3.2: Different monolith brick specifications.....	17
Table 3.3: Calculation of the feed velocity.....	18
Table 3.4- Typical values for some of important parameters at 450 K.....	32

## List of Figures

Figure 3.1: Schematic view of converter .....	16
Figure 4.1 - Pressure contours for cold flow through 400 CPSI std wall monolith at an inlet velocity of 7.6 m/s. The medium length converter is shown .....	33
Figure 4.2 - Pressure contours for cold flow through 400 CPSI std wall monolith at an inlet velocity of 15.11 m/s. The medium length converter is shown .....	34
Figure 4.3 - Pressure contours for cold flow through 400 CPSI std wall monolith at an inlet velocity of 30.22 m/s. The medium length converter is shown .....	34
Figure 4.4- Pressure drop of the monolith brick with respect to radial position. Velocity is changing from 0.02 kg/s (7.6 m/s) to 0.08 kg/s (30.22 m/s). Medium length converter is regarded. ....	35
Figure 4.5 - Pressure contours for cold flow through 400 CPSI std wall monolith at an inlet velocity of 15.11 m/s. The medium length converter is shown .....	36
Figure 4.6 - Pressure contours for cold flow through 400 CPSI thin wall monolith at an inlet velocity of 15.11 m/s. The medium length converter is shown .....	36
Figure 4.7 - Pressure contours for cold flow through 900 CPSI wall monolith at an inlet velocity of 15.11 m/s. The medium length converter is shown.....	37
Figure 4.7- Pressure drop of the monolith brick with respect to radial position for different monolith CPSI is the. Long length converter is regarded and inlet velocity is 15.11 m/s. ....	38
Figure 4.8- Pressure drop of the monolith brick in the monolith with respect to radial position. Inlet velocity is 15.11 m/s and monolith CPSI is 400 std. short, middle and long size converters is regarded. ....	39
Figure 4.9 -Axial velocity at the monolith entrance with respect to radial position. Short, middle and long converters are compared. Inlet velocity is 15.11 m/s and monolith CPSI is 400 std. ....	40

Figure 4.10 -Axial velocity at the monolith brick entrance with respect to radial position. Different monolith CPSI configurations are compared. Inlet velocity is 30.22 m/s and middle size model is shown.....	41
Figure 4.11 – Turbulent kinetic energy contours for cold flow through 400 CPSI thin wall monolith at an inlet velocity of 7.6 m/s. The long length converter is shown.....	42
Figure 4.12 – Turbulent kinetic energy contours for cold flow through 400 CPSI thin wall monolith at an inlet velocity of 15.11 m/s. The long length converter is shown.....	42
Figure 4.13 – Turbulent kinetic energy contours for cold flow through 400 CPSI thin wall monolith at an inlet velocity of 30.22 m/s. The long length converter is shown.....	43
Figure 4.14 – Turbulent kinetic energy contours for cold flow through 400 CPSI monolith at an inlet velocity of 30.22 m/s. The short length converter is shown .	44
Figure 4.15 – Turbulent kinetic energy contours for cold flow through 400 CPSI monolith at an inlet velocity of 30.22 m/s. The middle length converter is shown .....	44
Figure 4.16 – Turbulent kinetic energy contours for cold flow through 400 CPSI monolith at an inlet velocity of 30.22 m/s. The long length converter is shown ..	45
Figure 4.17- Axial velocity at the entrance of the monolith brick. Middle size model was chosen as the basis and inlet cone extended to 10 cm. monolith CPSI is 400 std and inlet velocity is 15.11 m/s.....	46
Figure 4.18 – Turbulent kinetic energy contours for cold flow through 400 CPSI monolith at an inlet velocity of 15.11 m/s. The middle length converter is shown .....	47
Figure 4.19 – Turbulent kinetic energy contours for cold flow through 400 CPSI monolith at an inlet velocity of 15.11 m/s. The middle length converter with extended inlet cone is shown.....	47
Figure 4.20- Pressure drop of monolith brick with respect to radial position. Middle size geometry and middle size with extended inlet cone are compared. Inlet velocity is 15.11 m/s and monolith CPSI is 400 std.....	48

Figure 4.21 – Temperature contours through 400 CPSI monolith at an inlet mass flow rate of 0.02 Kg/s. The middle length converter is shown.....	50
Figure 4.22 – Temperature contours through 900 CPSI monolith at an inlet mass flow rate of 0.02 Kg/s. The middle length converter is shown.....	50
Figure 4.23 – Temperature contours through 400 CPSI thin wall monolith at an inlet mass flow rate of 0.02 Kg/s. The middle length converter is shown.....	51
Figure 4.24- Average solid temperature of the monolith brick with time for a feed with 0.02 Kg/s mass flow rate. Different monolith CPSI configurations are compared. Middle size converter is shown.....	52
Figure 4.25- Average solid and fluid temperatures in the 400 CPSI with thin wall monolith brick with time for a feed with 0.02 Kg/s mass flow rate are shown. Middle size converter is shown.....	53
Figure 4.26- Average solid and fluid temperatures in the 900 CPSI monolith brick with time for a feed with 0.02 Kg/s mass flow rate are shown. Middle size converter is shown.....	53
Figure 4.27- Average solid and fluid temperatures in the 400 std CPSI monolith brick with time for a feed with 0.02 Kg/s mass flow rate are shown. Middle size converter is shown.....	54
Figure 4.28- Average solid temperature of the monolith brick with time for a feed with 0.02 Kg/s mass flow rate. Short, middle and long length converters are compared. Monolith brick CPSI is 400 std.....	55
Figure 4.29- Average solid and fluid temperatures in the 400 std CPSI monolith brick with time for a feed with 0.02 Kg/s mass flow rate are shown. Long and short length models are compared.....	56
Figure 4.30- CO Conversion for different monolith CPSI configurations. Inlet mass flow rate is 0.02 Kg/s. Middle size converter is considered.....	58
Figure 4.31- CO conversion for short, middle and long length converters. Inlet mass flow rate is 0.02 Kg/s and monolith brick is 400 CPSI std.....	59
Figure 4.32- CO conversion for different monolith CPSI configurations. Middle length converter is the basis and inlet cone extended from 5 cm to 10 cm. Inlet mass flow rate is 0.02 Kg/s.....	60

## Nomenclature

$A_0$	Pre-exponential factor
$a_v$	Surface to Volume ratio
$C$	Molar Density (Concentration), mol/m <sup>3</sup>
$C_{CO}$	Molar Density (Concentration) of CO, mol/m <sup>3</sup>
$C_f$	Total Molar Density (Concentration) of Fluid or Gas
$C_p$	Constant Pressure Specific Heat of Fluid or Gas, J/Kg.K
$C_\mu$	Constant
$C_{\varepsilon 1}$	Constant
$C_{\varepsilon 2}$	Constant
$D$	Diameter of channel or pipe, m
$D$	Diffusion Coefficient, m <sup>2</sup> /s
$D_{AB}$	Diffusion Coefficient, m <sup>2</sup> /s
$D_k$	Knudson Diffusion, M <sup>2</sup> /s
$D_{eff}$	Effective Diffusion Coefficient, m <sup>2</sup> /s
$D_H$	Hydraulic Diameter of Channel, m
$d_p$	Mean Pore Diameter, m
$E$	Activation Energy, J/mol
$\Delta H$	Enthalpy Change of Reaction, J/mol
$h$	Average convective heat transfer coefficient, W/m <sup>2</sup> .K
$k$	Thermal Conductivity of Fluid, W/m.K
$k$	Turbulent Energy, m <sup>2</sup> /s <sup>2</sup>
$k_f$	Thermal Conductivity of Fluid or Gas, W/m.K
$k_r$	Reaction Rate Constant, s <sup>-1</sup>
$k_{CO}$	Reaction Rate Constant, s <sup>-1</sup>
$k_{app}$	Apparent reaction rate, s <sup>-1</sup>
$k_{eff}$	Effective Thermal Conductivity of Solid, W/ (m.K)
$k_m$	Mass Transfer Coefficient, m/s
$L_C$	Characteristic Length of Washcoat, m
$M$	Molecular Mass of Species
$Nu$	Nusselt Number

$P$	Total Pressure, Pa
$R_g$	Gas Constant, J/mol K
$r$	Radial Coordinate in Cylindrical Coordinate System, m
$R_{CO}$	Reaction Rate of CO based on Washcoat Volume, mol/(m <sup>3</sup> .s)
$Sh$	Sherwood Number
$S$	Modulus of the Mean Rate-of-Strain Tensor
$t_c$	Washcoat thickness, m
$t_s$	Total Wall Thickness, m
$T$	Temperature, K
$T_f$	Temperature of Fluid or Gas, K
$T_s$	Surface Temperature, K
$V$	Velocity of Fluid or Gas, m/s
$v$	Velocity of Fluid or Gas, m/s
$Y_{CO}$	Mole Fraction of CO
$\nabla$	Gradient

### **Greek Letters**

$\rho$	Density of Fluid or Gas, m/s
$\rho_s$	Density of Solid (Washcoat or Substrate), kg/m <sup>3</sup>
$\varepsilon$	Dissipation Rate of Turbulent Energy, m <sup>2</sup> /s <sup>3</sup>
$\varepsilon_w$	Washcoat Porosity
$\varepsilon_s$	Solid porosity
$\varepsilon_m$	Monolith porosity
$\tau$	Tortuosity Factor
$\sigma_k$	Constant
$\sigma_\varepsilon$	Constant
$\eta$	Effectiveness factor
$\mu$	Kinematic Viscosity of Fluid or Gas, Pa-s
$\nu T$	Turbulent Viscosity of Fluid or Gas
$\Phi$	Thiele modulus

### **Subscripts**

$f$	Fluid Properties
-----	------------------

s	Solid Properties (Washcoat or Substrate)
eff	Effective property in mentioned medium
a	Axial direction
r	Radial direction

### **Abbreviations**

1D	One Dimensional
2D	Two Dimensional
3D	Three Dimensional
CPSI	Cell Per Square Inch
CPSM	Cell per Square Meter
GHSV	Gas Hourly Space Velocity
ppm	Parts Per Million
std	Standard
STP	Standard Temperature and Pressure

# Chapter 1

## Introduction

Fossil fuels, easy to harness and with widespread availability and reasonable price, have been the main source of energy in the last century. Although it is often predicted that oil resources will be soon depleted, the emergence of new exploration and production technologies, combined with the lack of a readily available and cost effective alternative, indicate that fossil fuels will continue to play a significant role in providing energy for the foreseeable future.

One of the main problems present in all areas of discovery, production, transportation and usage of petroleum and its products is the pollution generated. Although not considered that important in the early days, concern has increased rapidly in the 1970s, and has intensified recently with concerns of manmade global warming. Although the introduction of government regulations has led to much progress in pollution abatement, the regulations continue to become stricter.

Automobiles throughout the world are one of the primary consumers of fossil fuel. There has been a lot of effort made to replace this source of energy with so-called green energies such as electricity, solar energy and biodiesel, but fossil fuels have continued their major role in supplying energy in cars. Considering this dominant role, a lot of effort has been made to improve the usage of these fuels and make them cleaner in the last thirty years. To control emissions from combustion, catalytic converters have been used and improved over the last decades. There are major advantages in using this device which will be discussed in the following chapters. In brief, in a catalytic converter, a catalytic reactor is used to control undesirable engine emissions.

Catalytic converters have been extensively studied in the last several decades. There are many parameters involved in the design and performance of a converter, which should be considered when designing them so as to produce a reasonably priced product while maintaining the main objective of a converter, namely to meet the government mandated emission limits. With the introduction of newer and stricter regulations on gas emissions from engines and also with the development of simulation software and computing power, this area remains attractive for more work and study. The main objective of this thesis is the study of light off behavior of different converter designs with respect to geometry and structure of the catalyst. To do so, FLUENT was selected as the computational tool, and a 2D heterogeneous model was investigated.

The structure of the rest of the thesis is as follows. In Chapter 2, the principle topics in converter design and some basic concepts has been discussed. Also in this chapter, a brief summary of past works and literature review has been presented. In Chapter 3, the methodology and the development of the model are introduced. Chapter 4 deals with the simulation results and the comparison between different factors involved in each converter. In Chapter 5, conclusions and recommendations for future work have been made.

# Chapter 2

## Background

In the 1960s, concern over high levels of toxic emissions from automobiles and the resulting smog that was created, led to the enactment of increasingly strict regulations that gave limits to the amounts of carbon monoxide, hydrocarbons and oxides of nitrogen that could be emitted from cars. Initially, these limits could be achieved by modifications to engine design, but as the regulations became stricter, the adoption of exhaust gas after treatment devices became standard practice.

In more recent years, concerns about global warming have led to increased calls for the use of alternative fuels and for enhanced fuel efficiency. These objectives can both be achieved to some degree by the use of lean burn technology, especially with diesel fuel or natural gas. As discussed shortly, the use of lean burn technology gives rise to its own set of challenges, and places more demand on the design of the after treatment system.

### 2.1 Greenhouse gas concerns and global warming

It is been an issue of everyday news. Global warming and its drastic effects on the lives of us and future generation is not something that can be ignored. In the last years, the efforts and concerns regarding this fact has been raised. Human being's activities in the energy section, which is primarily based on fossil fuel combustion, is believed by many to be a prime cause of global warming. By releasing greenhouse gases from almost any activity which uses fossil fuels as a source of energy, human being contributes to a large amount of this global warming. According to IPCC (Intergovernmental Panel on Climate change) these

kinds of activities may lead to an average increase of air temperature between 1.1 to 6.4 °C in the twenty-first century. Considering that the global air temperature rise in the last century was estimated to be about  $0.74 \pm 0.18$  °C, this temperature increase, if it materialized, would affect the living condition of human beings drastically, and can lead to some severe results which may be irreversible. (“Summary of policymakers” by IPCC, 2007).

Among greenhouse gases, carbon dioxide (CO<sub>2</sub>), methane (CH<sub>4</sub>), and nitrous oxide (N<sub>2</sub>O) are the primary ones of concern which are produced each day from automobiles throughout the world. Note that although water is the most abundant greenhouse gas, it is not normally considered, because the water concentration in the atmosphere is believed to be constant. In 2002, the share of each gas in Canada’s greenhouse production was as follows: CO<sub>2</sub> (78%), CH<sub>4</sub> (12.6%) and N<sub>2</sub>O (7.4%). It is interesting to know that while CO<sub>2</sub> is the major emitting gas among all, methane emissions are as important as CO<sub>2</sub>. It is based on the fact that methane has a global warming potential (GWP) of 23 times that of carbon dioxide.

## **2.2 Catalytic converter**

Catalytic converters use combustion to control emissions of carbon monoxide and hydrocarbons, both produced by incomplete combustion in the engine. Two types of combustion can be used to decrease the amount of undesired pollutants in any industrial activity.

Homogeneous combustion is one of the main ways for pollution control. A typical use of this process is the flares widely used in oil and gas industry. Low cost and easy application of this type of combustion is one of its main advantages. But this type of combustion has some limitations which should be considered. Homogeneous combustion may lead to NO<sub>x</sub> production which cannot easily be ignored. Nitrogen oxides, NO and NO<sub>2</sub>, which are abbreviated as NO<sub>x</sub> are other

important pollutants that in any environmental application tried to be avoided. Furthermore, homogeneous combustion only occurs in well defined flammability limits, which restricts its use in automotive applications. Although there were some early attempts to use homogeneous combustion in exhaust gas after treatment devices, this approach has given way to catalytic systems. Homogeneous systems are also unable to eliminate  $\text{NO}_x$ , which was required as government regulations became stricter.

The other option for combustion for pollution control is catalytic combustion. Catalytic combustion is a flameless combustion process that can occur at relatively low temperatures. In this case, a catalyst is used to increase the rate of the oxidation (and also the reduction) reactions. First use of this kind of combustion can be traced back to early 19<sup>th</sup> century, when Sir Humphrey Davy discovered that methane and oxygen in the presence of hot platinum could react in a flameless way. After that, due to considerable advantages, catalytic combustion applications have grown its dominance in industry.

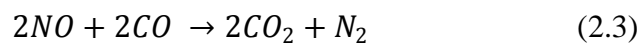
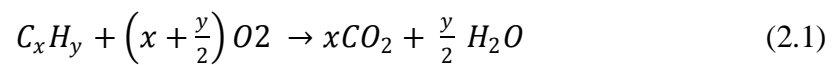
There are some advantages regarding the use of catalytic combustion. One of the main advantages is that this type of combustion can occur in low temperatures and there is no need for high temperature for igniting the gas and generating flame. The ability to use this type of combustion for any feed concentration is another important advantage which makes catalytic combustion favorable with respect to homogeneous combustion.

From 1966 on, which was the first time that exhaust emission was regulated, the allowable amount of the polluting gases from exhaust pipes in automobiles has become considerably stricter. At that time, regulation was concerned only with CO and HC (hydrocarbons) emissions from motor vehicles. Early emission limits could be met with improved engine design, but with the legislation of Clean Air Act on 1970 in the US, and more strict regulation for HC, CO and also  $\text{NO}_x$  emissions, the necessity of more efficient treatment of exhaust gases emerged. In the 1970s, catalytic converters became an interesting topic and they continued

their major role of pollution control in automobiles afterwards. Although homogeneous combustion first tried to satisfy the new regulations on vehicles, their serious limitations caused them to lose in the rivalry with new and more effective catalytic converters, which were more adaptable with the condition of engine gases, i.e. low temperature. Nowadays, this type of converter is the only commonly used type in cars (Hayes et al., 1997).

There are two main types of catalytic after treatment systems. The choice of system depends on the mode of engine operation. For most gasoline engines, the engine is operated in stoichiometric mode, which means that sufficient oxygen is admitted with the fuel to provide for complete combustion, with no excess oxygen. For most Diesel engines, many natural gas engines, and some gasoline engines, excess air is admitted with the fuel, and thus this mode is referred to as lean operation.

For stoichiometric operation, the three way catalyst is usually used. This catalyst oxidizes CO and HC and reduces NO<sub>x</sub>. Although the reaction scheme is somewhat complex, in simple form it can be represented by the following three main overall reactions:



For lean burn engines, the presence of excess oxygen in the exhaust gas prevents the reduction of  $\text{NO}_x$  and three way converters cannot meet the regulations and limits. In this type of after treatment system, the first converter oxidizes CO, HC and NO, and additional reactors are used to reduce the  $\text{NO}_x$ , using one of several options. Examples of these include the lean  $\text{NO}_x$  traps and the selective catalytic reduction systems (SCR).

### **2.2.1 Monolith converters**

The catalyst used in the converter is a noble metal or metals, usually platinum, palladium and rhodium. Other materials may also be added, such as ceria in three way catalysts added as an oxygen storage component, and barium compounds, used in  $\text{NO}_x$  storage traps. Regardless of the active components, they are combined with a support, to give a supported metal catalyst. This arrangement is typical of many industrial catalysts. The supported catalyst must be incorporated into the reactor (converter). Early converters used a packed bed, in which pellets of supported catalyst were used, either as a random packed bed or with pellets supported on wire screens. These structures proved to be unsatisfactory, partly due to the harsh conditions of the automobile in use. Packed beds suffered from problems of gas bypassing and attrition of the particles owing to vehicular motion. Today, the monolith design is dominant. The monolith reactor is a type of reactor which consists of several thousands of very small and narrow channels. In these channels, gas flows and reacts with the catalyst which is placed on the walls of each channel. On the walls of each channel a porous layer is coated which is called washcoat. Catalyst is dispersed on the washcoat. This type of design has advantages which resulted in early attention of major car companies to it. Low pressure drop as well its unique stable design and very high surface to volume ratio can regard as some of its advantages.

Circular, square, triangular, hexagonal or sinusoidal in shape (Bhattacharya et al., 2004) and ceramic or metallic alloys in material, they can be made with a broad range of wall thickness, cell density and specific size.

Based on the temperature and catalyst used, there is quite a broad selection for the monolith substrate material. Ceramic, mainly Cordierite, is very common, and metal alloys such as ferralloy steel is also widely used. As mentioned before, the surface of the substrate is coated with a porous material which is called washcoat. The active catalyst is dispersed in the washcoat. The role of washcoat is to generate a high surface area so that reaction takes place effectively. The thickness of washcoat is between 10  $\mu\text{m}$  and 150  $\mu\text{m}$ . Gamma alumina ( $\gamma\text{-Al}_2\text{O}_3$ ) is a commonly used washcoat material used in converters.

The diameter of each monolith channel is small, typically of the order of 1 mm. Different designs have different diameters and it is important to know that even very small variations in hydraulic diameter of a monolith channel can have great impacts on a performance of a catalytic converter. The most commonly used monolithic catalyst converter uses a ceramic substrate with square channels and having 400 cells per square inch of frontal area (CPSI). To overcome some operational problems, as discussed shortly, some monoliths use a higher cell density, such as 900 CPSI, or use a thinner wall. The choice of substrate configuration ultimately depends on the desired operational performance.

Mass and heat transfer considerations are of high importance in any study on catalytic converters. When fluid containing reactants moves along the channels in the converter, molecular diffusion from bulk to the surface of the washcoat occurs. This type of mass transfer is called external mass transfer and is regarded as one of the limiting factor in the rate of the reaction. Also, another type of mass transfer occurs when reactant diffuse from the surface of the washcoat through the pores containing the catalyst. This type of mass transfer is called internal mass transfer and in many situations can be the main rate limiting factor. Considering Chilton-Coburn analogy, the same behavior can be regarded for heat transfer.

These two important factors, heat and mass transfer, should be applied in any simulation of the catalytic converter.

The cold start period, which is defined as the period when the engine is turned on, and the converter is cold, until the converter reaches its operating temperature, is of key importance in the operational cycle because this period corresponds to the one in which the majority of the emissions can occur. One of the main variables used to characterize the converter operation is the so-called light-off temperature. By definition, the light-off temperature corresponds to the inlet temperature at which 50 % of the reactant in question is converted to products. A key design objective is to have as low a light-off temperature as possible. The light-off temperature depends on the operating conditions such as emission concentration, ambient temperature, etc.

In general, there are regions in the behavior of a converter after cold start. In the first stage, gas inlet temperature is low and therefore the rate of the reaction is limited. This step has low conversion and is due to the fact that intrinsic rate of reaction is slower than mass transfer step in channels, it is called kinetically controlled regime. The second stage is called the ignition (or light-off) stage. In this stage, temperature begins to rise, catalyst begins to be activate and diffusion rate is also much bigger than previous stage. In this stage, light-off occurs and the rate of the reaction increases rapidly due to Arrhenius temperature dependant term in the rate equation. The third stage occurs afterwards. In this regime, temperature is high and therefore high conversion of the reactants occurs in the converter. In this stage, mass transfer often controls the overall rate of the reaction and acts as a limiting factor. This stage is also called mass transfer controlled regime.

## **2.3 Modeling of monolith converters**

Computer modeling has been used in the area of the catalytic converter from its early days of development. There are several advantages in using a computer

model compared to using only experimental design. The computer simulation allows for the relatively rapid testing of many scenarios that would be costly to perform experimentally. The computer modeling can be used to eliminate potentially unsatisfactory options, and generally speed the development process. The increase in power, coupled to the large decrease in cost of computers in the last two decades has had an important role in defining new models and more rigorous studies on this area. Developing of the models from early 1D studies to 2D or 3D, considering mass and heat transfer effects on single or continuum models and developing several new simulation software with less time consuming feature has helped scholars to investigate many of the parameters governing the performance of catalytic converter in a more detailed and rigorous way. There are many ways to model a converter. One chooses his own model based on the assumptions and the area he needs to focus on.

Although there are many different types of models, they can generally be divided into two main types. For a monolith type reactor, these are known as single channel models (SCM) or full converter models (FCM). In the SCM, a single channel of the monolith honeycomb is considered. There are many different levels of approximation that can be made in these models. If all channels are considered to have the same behaviour, then the performance of the single channel would be representative of the reactor as a whole. Normally, there are flow variations as well as radial temperature gradients, and therefore a single channel model is unlikely to represent the behaviour of the entire converter. In this case, a FCM can be used to predict flow maldistribution and other type of non-uniform behaviour.

When choosing a model and considering the assumptions to be made, there will always be a trade-off between time and accuracy. A simple model requires less execution time but may yield less accurate results, although the model may be sufficient. Although there are a wide variety of models resulting from different assumptions, there are a few features of all models that are worth discussing.

A key decision that affects computational requirements is the number of space dimensions used in the model. A SCM can have one, two or three space dimensions. A one dimensional model ignores the radial gradients in all variables, and assumes a plug flow. This will cause some inaccuracies, because the laminar flow in the channels will have a radial profile. A two dimensional model allows for the treatment of radial gradients, but assumes axi-symmetry. This assumption requires that the channels be approximated by right circular cylinders. The most accurate model would be a three dimensional model that accounts for the actual channel shape. The 3D model is quite expensive to run, and is not used very often. For a FCM, a 1D model would be in effect a single channel model, and thus is not used. The reason for using a FCM is allow for channel variation and hence radial profiles, thus either 2D or 3D models are used, the choice depending on whether or not the converter has axi-symmetry.

The second major characterization of converter models is the division into discrete or continuum models. In a discrete model, the solution is resolved at the scale of the real physical structure of the monolith; that is, all of the fluid and solid domains are retained, and the conservation equations solved for each one. SCM are usually discrete models, and the fluid and solid phases are both modeled. For a FCM, the use of a discrete model makes an extremely large problem, which it is not currently possible to solve using conventional numerical methodologies. The approach normally adopted is to use a continuum model, in which the porous monolith is assumed to be a continuous medium, albeit one consisting of two phases. In this approach, a volume averaging method is used to develop appropriate equations of conservation.

In another categorization, two types of modeling can be used regarding the number of phases considered in the converter. In pseudo-homogeneous modeling, fluid and solid are regarded as one phase and average properties of solid and fluid are applied. This simplification treats both phases as one phase and uses a unique temperature and concentration for both. This approximation can give unacceptable results in some cases. When an exothermic reaction occurs in the

system, there will be temperature difference between solid and fluid. This temperature difference may be significant. Especially when there is a relatively high concentration of the reactants or there are large changes in inlet conditions. In the other approach to the modeling, two separate phases are considered. In this type of modeling, solid and fluid are assigned different properties and the relation between different phases are defined by mass and heat transfer coefficients. These models are called heterogeneous models and usually give more accurate results.

In the last decades, a lot of studies on the modeling and simulation of catalytic converters has been done. Models with different level of complexity for both steady state and transient modes have been developed and studied.

Single channel models were studied in early days of catalytic converter usage due to its simplicity. Early modeling and simulations of monolithic reactor using one dimensional two phase models and two dimensional models with radial gradients discussed by Heck et al.(1976) and Young and Finlayson (1976). First models used adiabatic and isothermal condition for the converter. Oh et al. (1978) presented Co and H<sub>2</sub> oxidation in monoliths and Boersma et al. (1978) and Hegedus et al. (1977) investigated on velocity and concentration profiles in the converter. From then, a lot of studies have been done on single channel modeling considering different parameters involved such as model dimension, Young and Finlayson (1976) , Lee and Aris (1977) , Otto and LeGray (1980); mass and heat transfer coefficient, Oh and Cavendish (1982), Zygorakis (1993), Tronoconi and Forzatti (1992); and geometry effect, Ramanathan et al. (2004), Hayes et al. (2004). Chen et al. (2008) presented a detailed review of different types of modeling of a single channel reactor and the effect of each parameter such as, internal and external diffusion, heat transfer effects, flow uniformity and reaction kinetics on the performance of the converter.

Multi-channel models, (Tischer et al. 2001; Groppi and Tronconi, 1996; Windmann et al.2003, Jahn et al. 1997) use a few channels and with intrapolation, the whole behavior of catalytic converter is modeled. Charkravarthy et al. (2002)

presented a multi-channel transient 2D model to study on flow non-uniformity effects on light-off behavior. The effect of mass flow rate and inlet gas temperature on index of uniformity and consequently on the light-off behavior and conversion performance of the catalytic converter was discussed.

The focus in this thesis is on continuum model ( Zygourakis, 1989; Luoma and Smith, 1996) which uses a volume averaging process to model the converter. Luoma and Smith (1996), Taylor (1999), Bezzo et al. (2000), Raja et al. (2000), Tsinoglou et al.( 2004), Bezzo et al. (2005), have used CFD codes to implement reaction, momentum, mass and heat balance in the converter. Due to being computationally expensive, full use of CFD codes in converter modeling, Tsinoglou et al.( 2004), Bezzo et al. (2005), is not prevalent. Simulation software using CFD codes such as FLUENT has been used in 2D or 3D modeling of the converter, Bezzo et al. (2000). In the following, some of the most related literature to this study has been briefly discussed.

Taylor (1999) presented a CFD-based model to study on the effects of heat and mass transfer in the monolith, heat generation and heat loss, and reactions occurring in the monolith. The effect of these parameters on the performance of the converter has been discussed.

Tsinoglou et al (2003) studied the transient behavior of a 2D model using flow resistant model (FRM). They discussed about the effect of the inlet cone on flow patterns in the converter and transient heat transfer inside the converter without any reaction.

Shi-jin et al. (2000) investigated on the effect of the inlet cone on flow distribution and pressure drop in the monolithic converter with isothermal condition and no reaction occurring. They also discussed about the use of two monolith brick with a gap in between and its effect on flow distribution in the converter. Jeong and Kim (1998) presented a 3D transient model to study on the effect of flow maldistribution on the light-off behavior of a monolithic converter.

They applied a heterogeneous approach to monolith brick and inlet cone and inlet pipe diameter effect on the light-off behavior of different species have been studied.

Zygourakis (1989) discussed the effect of flow distribution profiles on the light-off behavior of a catalytic converter. He used a transient 2D model with heterogeneous approach for monolith brick and applied Voltz et al (1973) model for CO combustion. The effect of different patterns for gas flow (parabolic, uniform and pinwheel) on light-off and ambient heat transfer was presented.

Martin et al. (1998) presented study state and transient behavior of the converter and the effect of maldistribution of flow on light-off and final conversion of a catalyst in ECE and EUDC test cycles.

Liu and Hayes (2006) presented a 3D model using both pseudo-homogeneous and heterogeneous model for monolith brick in FLUENT context. Methane ignition and CO combustion in a reverse flow catalytic reactor and the comparison between homogeneous and heterogeneous models for monolithic section has been studied.

# Chapter 3

## Model development and methodology

### 3.1 Model characteristics

As noted earlier, the objective of this investigation was to study the effect of monolith geometry on the temperature distribution and light-off characteristics. The modeling domain consisted of the monolith brick and the inlet and outlet sections that represent the attachment to the exhaust system. The model selected was a two dimensional axisymmetric representation, and used a heterogeneous continuum model. The schematic view of the design is shown in Figure 3.1. In all simulations, the volume of the monolithic section, which is total reaction volume, was set to be  $2.15 \times 10^{-3} \text{ m}^3$ . Different geometries and shapes were used for comparison purposes which will be discussed in detail in the following.

#### 3.1.1 Geometry

Three different sizes for the converter were considered, referred to as short, middle and long. All three sizes had the same volume of  $2.15 \times 10^{-3} \text{ m}^3$ . In Table 3.1 details of different sizes of the converter is come.

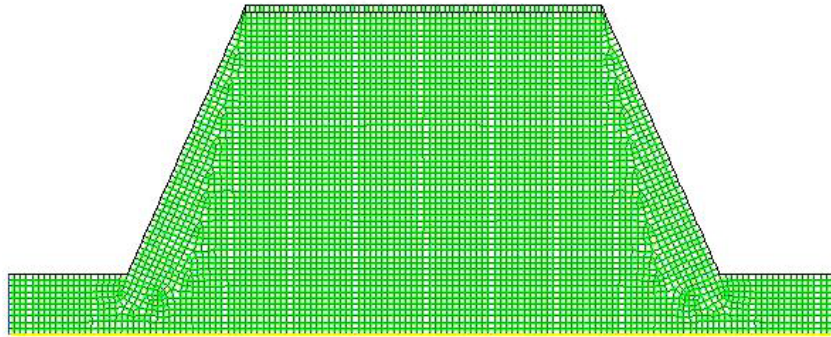


Figure 3.1: Schematic view of converter

Size	monolith brick length	monolith brick diameter	inlet pipe diameter	converter length
short	10	16.55 (cm)	2.5 (cm)	30 (cm)
middle	15	13.51 (cm)	2.5 (cm)	35 (cm)
long	20	11.70 (cm)	2.5 (cm)	40 (cm)

Table 3.1- Sizing specification of the modeled converters

### 3.1.2 Monolith properties

In all simulations, three different type of monolith substrate were used. These were all based on ceramic substrates available commercially. The first is the very commonly used 400 cells per square inch (CPSI) with standard wall thickness. The second was a 400 CPSI monolith with thin walls, and the third was a 900 CPSI monolith. The same amount of washcoat volume was used in all three

substrates. The dimensions and physical properties of the three substrates is presented in Table 3.2.

Properties	400 CPSI	400-thin CPSI	900-thin CPSI
<b>CPSM</b>	6.20E+05	1.40E+06	6.20E+05
<b>total wall thickness (<math>t_s</math>)</b>	0.1778 mm	6.35e-2 mm	6.35e-2 mm
<b>substrate volume fraction</b>	0.26	0.144	0.0975
<b>washcoat volume fraction</b>	0.12	0.12	0.12
<b>fluid volume fraction</b>	0.62	0.736	0.7825
<b>washcoat thickness (<math>t_c</math>)</b>	46 $\mu\text{m}$	28.4 $\mu\text{m}$	41.5 $\mu\text{m}$
<b><math>D_H</math></b>	1.0002 mm	0.7264 mm	1.1234 mm
<b><math>B_s</math></b>	1.0922 mm	0.7832 mm	1.2065 mm
<b>bulk density(substrate)</b>	464 $\text{kg/m}^3$	257 $\text{kg/m}^3$	174 $\text{kg/m}^3$
<b>bulk density(final)</b>	596 $\text{kg/m}^3$	389 $\text{kg/m}^3$	306 $\text{kg/m}^3$
<b>axial permeability (<math>\text{m}^2</math>)</b>	1.94E-08	3.09E-09	1.21E-08

Table 3.2: Different monolith brick specifications

Also, for the housing of the converter, the properties of Steel have been used and the following properties are regarded for insulating material:

$$\rho = 600 \quad \text{Kg/m}^3$$

$$C_p = 300 \quad \text{J/ Kg.K}$$

$$k = 0.2 \quad \text{W/m.k}$$

### 3.1.3 Feed properties

In this study, a typical feed with 10% Oxygen and 1000 ppm CO has been regarded. This feed enters the converter with three different rates; which are 0.02,

0.04 and 0.08 Kg/s. In all cases, Reynolds number at the inlet pipe of the converter is high enough to put it in turbulent regime. k-ε model has been used for the flow in the inlet section of the converter. Table 3.3 gives much detail about the velocity of the feed in the converter.

Feed mass flow rate (Kg/s)	GHSV (h <sup>-1</sup> )	inlet velocity at STP (m/s)
<b>0.02</b>	25000	7.6
<b>0.04</b>	50000	15.11
<b>0.08</b>	10000	30.22

Table 3.3: Calculation of the feed velocity

### **3.2 Mathematical model for kinetics with internal and external mass transfer**

As discussed in Chapter 2, the reactions occurring within a catalytic converter are complex. To focus attention on the geometrical aspects of the problem, and to make the simulations faster and more tractable, a single reaction was used for illustration purposes. The kinetic model was taken to be first order, which for the easy implementation of both internal and external mass transfer effects. The model reaction chosen was the oxidation of CO, which is one of the most important reactions in the converter.

### 3.2.1 Kinetic equation

The first order rate equation for the oxidation of CO in an excess of oxygen can be written as:

$$(-R_{CO}) = k_R C_{CO} = A_0 \exp\left(\frac{-E}{R_g T}\right) C_{CO} \quad (3.1)$$

The reaction rate in this equation is based on the washcoat volume. Because a continuum model was used in this work, the rate is scaled by the fraction of the volume occupied by the washcoat. The conservation equations (given shortly) are based on the entire volume. The rate implemented in the continuum model is thus:

$$(-R_{CO}) = \varepsilon_W A_0 \exp\left(\frac{-E}{R_g T}\right) C_{CO} = \varepsilon_W A_0 \exp\left(\frac{-E}{R_g T}\right) C Y_{CO} \quad (3.2)$$

where  $\varepsilon_W$  is the fraction of the reactor volume occupied by the washcoat. The fluid can be treated as an ideal gas with mass and molar densities given by:

$$\rho = \frac{\bar{M} P}{R_g T} \quad \text{and} \quad C = \frac{P}{R_g T} \quad (3.3)$$

### 3.2.2 Internal mass transfer

The reaction occurs within the porous washcoat structure. To gain access to the active catalytic sites, the reactants must propagate by diffusion into the washcoat. The actual rate within the washcoat is thus different from the value of the rate calculated at the surface of the washcoat. This internal diffusion resistance can be incorporated using an effectiveness factor. The reaction rate in terms of mole fraction at the catalyst external surface and the effectiveness factor is:

$$(-R_{CO}) = \varepsilon_W \eta A_0 \exp\left(\frac{-E}{R_g T_s}\right) C Y_{CO,s} \quad (3.4)$$

The effective diffusion coefficient in the pores depends on both the Knudsen and bulk diffusivity, however Knudsen diffusion dominates. The Knudsen diffusion coefficient is:

$$D_K = 48.5 d_p \left(\frac{T}{M}\right)^{0.5} \quad (3.5)$$

M is the molar mass of the diffusing component, T is the temperature (K), and  $d_p$  is the pore diameter in m. the effective diffusivity depends on the catalyst porosity,  $\varepsilon$ , and tortuosity,  $\tau$ .

$$D_{eff} = \frac{\varepsilon}{\tau} D_K \quad (3.6)$$

where for a first order reaction, the generalized Thiele modulus is:

$$\Phi = L_C \sqrt{\frac{k_R}{D_{eff}}} \quad (3.7)$$

We use the generalized effectiveness factor, where the characteristic length,  $L_C$ , is defined as the washcoat volume divided by the external surface area. For a washcoat approximated as an annular section in a channel of hydraulic diameter  $D_H$  and washcoat thickness  $t_C$ , the characteristic length is:

$$L_C = t_C \left(1 + \frac{t_C}{D_H}\right) \quad (3.8)$$

The generalized effectiveness factor for an isothermal first order reaction is:

$$\eta = \frac{\tanh(\Phi)}{\Phi} \quad (3.9)$$

### 3.2.3 External mass transfer

The external transport resistance is also important. The rate in the bulk phase can be related to the rate at the catalyst surface by equating the rates of mass transfer and reaction.

$$k_m a_v C_f (Y_{CO,f} - Y_{CO,s}) = \varepsilon_W \eta A_0 \exp\left(\frac{-E}{R_g T_S}\right) C Y_{CO,s} \quad (3.10)$$

Rearrange to give the relationship between the concentration in the fluid and at the solid surface:

$$Y_{CO,f} = \left(\frac{\varepsilon_W \eta k_r C_S + k_m a_v C_f}{k_m a_v C_f}\right) Y_{CO,s} \quad (3.11)$$

The reaction rate can be written using the bulk fluid concentration and an apparent rate constant:

$$(-R_{CO}) = k_{app} C_{CO,f} = k_{app} C_f Y_{CO,f} \quad (3.12)$$

If we substitute the rate for the surface concentration by the bulk fluid concentration we get:

$$(-R_{CO}) = \frac{\varepsilon_W \eta k_r}{\left(\frac{\varepsilon_W \eta k_r C_S + k_m a_v C_f}{k_m a_v C_f}\right)} C_S Y_{CO,f} = \frac{\varepsilon_W \eta k_r}{\left(\frac{\varepsilon_W \eta k_r C_S + k_m a_v C_f}{k_m a_v C_S}\right)} C_f Y_{CO,f} \quad (3.13)$$

Therefore the apparent reaction rate is seen to be given by:

$$k_{app} = \frac{\varepsilon_W \eta k_r}{\left(\frac{\varepsilon_W \eta k_r C_S + k_m a_v C_f}{k_m a_v C_S}\right)} = \frac{(\varepsilon_W \eta k_r)(k_m a_v C_S)}{\varepsilon_W \eta k_r C_S + k_m a_v C_f} \quad (3.14)$$

Note that:

$$\frac{C_f}{C_S} = \frac{T_S}{T_f} \quad (3.15)$$

Then we can rearrange:

$$\frac{1}{k_{app}} = \frac{1}{\varepsilon_W \eta k_r} \frac{T_S}{T_f} + \frac{1}{k_m a_v} \quad (3.16)$$

Note again that the rate constant  $k_R$  is evaluated at the surface temperature. The area to volume ratio for a monolith is calculated using the fractional open frontal area, or porosity, of the monolith structure and the hydraulic diameter of the channels.

$$a_v = \frac{4\varepsilon_S}{D_H} \quad (3.17)$$

The mass transfer coefficient is computed from the Sherwood number:

$$Sh = \frac{k_m D_H}{D_{AB}} \quad (3.18)$$

The use of the apparent rate constant allows for the reaction rate to be expressed in terms of the bulk fluid concentration. The binary diffusion coefficient for CO in air is:

$$D_{AB} = 9.15 \times 10^{-10} T^{1.75} \quad (3.19)$$

### 3.2.4 Parameter values for the study

The parameters to use for the rate model are:

$$(-R_{CO}) = A_0 \exp\left(\frac{-E}{R_g T}\right) C Y_{CO} = 7 \times 10^{15} \exp\left(\frac{-12118}{T_S}\right) C Y_{CO} \quad (3.20)$$

These parameters were chosen based on typical literature values for the reaction rate for typical catalytic converters. For all of the substrate geometries, the fraction of the reactor volume occupied by the washcoat,  $\varepsilon_w$ , is 0.12. The Knudsen diffusion coefficient for CO is based on a mean pore diameter of 10 nm and the molecular mass of 28 to give:

$$D_K = 9.17 \times 10^{-8} (T)^{0.5} \quad (3.21)$$

The washcoat porosity used was 0.5 and a tortuosity factor was 0.5, so that the effective diffusivity is given by:

$$D_{eff} = 9.17 \times 10^{-8} (T)^{0.5} \frac{m^2}{s} \quad (3.22)$$

The parameters required to compute the characteristic washcoat length and other mass transfer parameters for the three substrates are given in Table 3.2.

### 3.3 The conservation equations

The simulation of the converter requires the solution of the conservation equations for the solution domain. The equations required are momentum balances for the monolith and the open sections, a mole balance for the fluid phase, and energy balances for the fluid and solid phases. Note that a mole balance for the solid phase is not explicitly required, because the first order reaction rate is written in terms of the bulk fluid concentration. In the following sections the conservation equations are given for an axi-symmetric domain.

#### 3.3.1 Momentum balances

Following the work of Liu et al. (2006), in this study, for monolith brick, solid and empty parts different momentum balance equations are discussed in the following.

##### 3.3.1.1 Empty sections

Inlet and outlet cones are the empty parts. In these regions flow is turbulent and Reynolds averaged Navier-Stokes equations were used to describe the flow. The continuity and Reynolds average Navier-Stokes equations are:

$$\frac{\partial \rho_f}{\partial t} + \nabla \cdot (\rho_f \tilde{v}) = 0 \quad (3.23)$$

$$\frac{\partial \rho_f \tilde{v}}{\partial t} + \nabla \cdot (\rho_f \tilde{v} \tilde{v}) = -\nabla p + \nabla \cdot \tilde{\tau} + \rho_f \tilde{g} + \tilde{F} - \nabla \cdot (\rho_f \overline{v'v'}) \quad (3.24)$$

The added term on the Reynolds-averaged transport equation account for the

turbulence. To solve the problem, this new variable should be determined. Eddy viscosity model is the most common relation to determine the added turbulent-related term. It is based on the Boussinesq assumption that turbulent stress tensor can be expressed in the term of the mean rate of strain. In this assumption, coefficient of molecular viscosity is replaced by turbulent stress and the mean rate of stress is treated in the same way as the viscous stress for Newtonian isotropic fluid. The turbulent stress is:

$$\rho_f \overline{v'v'} = -\tilde{\tau}_t = \frac{2}{3}kI - \mu_t(\nabla\tilde{v} + \nabla\tilde{v}^T) \quad (3.25)$$

This formula, based on the way that turbulent viscosity,  $\mu_t$ , is calculated, is used for a broad range of turbulent models. To calculate turbulent viscosity, the most widespread model is the standard  $k$ - $\varepsilon$  model. The standard  $k$ - $\varepsilon$  model is based on model transport equations for the turbulent kinetic energy ( $k$ ) and its dissipation rate ( $\varepsilon$ ).  $k$  is the first transported variable and accounts for the energy in the turbulence.  $\varepsilon$  is the second transported variable and accounts for the turbulent dissipation. The turbulent kinetic energy,  $k$ , and its rate of dissipation,  $\varepsilon$  are obtained from the following transport equations:

$$\frac{\partial(\rho_f k)}{\partial t} + \frac{\partial(\rho_f k u_i)}{\partial x_i} = \frac{\partial}{\partial x_i} \left[ \left( \mu + \frac{\mu_t}{\sigma_k} \right) \frac{\partial k}{\partial x_i} \right] + G_k + G_b - \rho_f \varepsilon \quad (3.26)$$

$$\frac{\partial(\rho_f \varepsilon)}{\partial t} + \frac{\partial(\rho_f \varepsilon u_i)}{\partial x_i} = \frac{\partial}{\partial x_i} \left[ \left( \mu + \frac{\mu_t}{\sigma_\varepsilon} \right) \frac{\partial \varepsilon}{\partial x_i} \right] + C_{1\varepsilon} \frac{\varepsilon}{k} (G_k + C_{3\varepsilon} G_b) - C_{2\varepsilon} \rho_f \frac{\varepsilon^2}{k} \quad (3.27)$$

The turbulent viscosity,  $\mu_t$ , is calculated from the following relation as follows:

$$\mu_t = \rho_f C_\mu \frac{k^2}{\varepsilon} \quad (3.28)$$

The constants in equations (3.26) and (3.27) are as follows:

$$C_{1\varepsilon} = 1.44, \quad C_{2\varepsilon} = 1.92, \quad C_\mu = 0.09, \quad \sigma_k = 1.0, \quad \sigma_\varepsilon = 1.3$$

These values have been found to work well for a wide range of flows.

$G_b$  accounts for the effects of buoyancy and is neglected.  $G_k$  which is the production of turbulent kinetic energy is calculated from:

$$G_k = -\rho \overline{v'v'} \frac{\partial u_j}{\partial x_i} \quad (3.29)$$

$G_k$  can be calculated from:

$$G_k = \mu_t S^2 \quad (3.30)$$

In the equation (3.30),  $S$  is the modulus of the mean rate-of-strain tensor, and is defined as  $S = \sqrt{2S_{ij}S_{ij}}$ . The mean strain rate  $S_{ij}$  is:

$$S_{ij} = \frac{1}{2} \left( \frac{\partial u_j}{\partial x_i} + \frac{\partial u_i}{\partial x_j} \right) \quad (3.31)$$

By using an analogy we can model turbulent mass and energy transfer. In this regard, turbulent mass and energy transfer and turbulent momentum transfer are supposed to have the same behavior. The effective dispersion coefficient and apparent thermal conductivity are, respectively:

$$D = D_{i,m} + \frac{\mu_t}{Sc_t} \quad (3.32)$$

$$k_{tur} = k_f + \frac{C_p \mu_t}{Pr_t} \quad (3.33)$$

### 3.3.1.2 Monolith section

In the monolith channels flow is laminar. The Navier-Stokes equation is used for momentum balance. Volume average approach is used for continuum model, and as far as solid is present in the system, extra terms are introduced. So continuity equation remains the same:

$$\frac{\partial \rho_f}{\partial t} + \nabla \cdot (\rho_f \vec{v}) = 0 \quad (3.34)$$

The velocity which is used is the superficial velocity, which is velocity multiplied by the porosity. The volume average Navier-Stokes is:

$$\frac{\partial}{\partial t}(\rho_f \vec{v}) + \nabla \cdot (\rho_f \vec{v} \vec{v}) = -\nabla P + \nabla \cdot (\bar{\tau}) + \rho_f \vec{g} + S_i \quad (3.35)$$

The source term,  $S_i$ , introduced for the porous medium can be defined in the form (Hayes et al. 1996; Hayes et al., 1997):

$$S_i = -\left(\frac{\mu}{K} v_i + C_2 \frac{1}{2} \rho_f |v| v_i\right) \quad (3.36)$$

The first term on the right hand side accounts for the viscous loss. This term is Darcy term and  $K$  is the medium permeability. For monolithic structure, due to very small diameter and the assumption of one dimensional flow,  $K$  is only regarded in flow direction. For radial direction (perpendicular to flow direction),  $K$  is set to a very small number to preserve this condition. The second term represents the inertial loss. For laminar flow through porous media, the inertial loss is negligible and can be neglected.

### 3.3.2 Mole balance fluid

The fluid phase mole balance in axi-symmetric coordinates for a monolith with an apparent first order reaction is:

$$\begin{aligned} \frac{1}{r} \frac{\partial}{\partial r} \left( r D_{r,eff} C_f \frac{\partial Y_{CO,f}}{\partial r} \right) + \frac{\partial}{\partial z} \left( D_{a,eff} C_f \frac{\partial Y_{CO,f}}{\partial z} \right) - v_s C_f \frac{\partial Y_{CO,f}}{\partial z} \\ - k_{app} C_f Y_{CO,f} = 0 \end{aligned} \quad (3.37)$$

Diffusion of mass occurs only in the axial direction, and not through the channel walls in the radial direction. The radial diffusion coefficient is thus set equal to zero and the equation simplifies to:

$$\frac{\partial}{\partial z} \left( D_{a,eff} C_f \frac{\partial Y_{CO,f}}{\partial z} \right) - v_s C_f \frac{\partial Y_{CO,f}}{\partial z} - k_{app} C_f Y_{CO,f} = 0 \quad (3.38)$$

In the axial direction, the diffusion is also small, but it can be approximated by the Taylor-Aris model for laminar flow, where:

$$D_{a,eff} = D_{AB} + \frac{(v D_H)^2}{196 D_{AB}} \quad (3.39)$$

### 3.3.3 Energy balances

The energy balance for the fluid includes the effects of axial flow, convection, and conduction. The energy accumulation in the fluid is small compared to the solid and the accumulation term in the fluid phase is dropped. In the fluid only the axial conduction term is retained.

$$\varepsilon_S \frac{d}{dz} \left( k_{af,eff} \frac{dT_f}{dz} \right) - v_s \rho_f C_{P,f} \frac{dT_f}{dz} + h a_v (T_S - T_f) = 0 \quad (3.40)$$

The energy balance in the solid phase is considers the effects of accumulation, axial conduction, radial conduction, convection, and energy generation by the reaction, as necessary. The form of the equation is:

$$\begin{aligned} \frac{1}{r} \frac{\partial}{\partial r} \left( r k_{rs,eff} \frac{\partial T_s}{\partial r} \right) + \frac{\partial}{\partial z} \left( k_{as,eff} \frac{\partial T_s}{\partial z} \right) + h a_v (T_S - T_f) + (1 - \varepsilon_S) \Delta H_R \eta (-R_{CO}) \\ = (1 - \varepsilon_S) \rho_S C_{P,S} \frac{\partial T_S}{\partial t} \end{aligned} \quad (3.41)$$

In a monolith, the effective thermal conductivity of the solid is a function of the porosity in the axial direction and a function of the monolith structure in the radial direction, thus:

$$k_{as,eff} = k_s (1 - \varepsilon_S) \quad \text{and} \quad k_{rs,eff} = k_s G \quad (3.42)$$

The factor G accounts for the structure of the monolith in the radial direction. The enthalpy of reaction is equal to:

$$\begin{aligned} (\Delta H^\circ_R)_{CO} = -279.581 - 1.861 \times 10^{-2} T + 2.52 \times 10^{-5} T^2 - \\ 1.2247 \times 10^{-8} T^3 + 2.255 \times 10^{-12} T^4 \end{aligned} \quad (3.43)$$

### **3.4 Implementing the model in FLUENT**

To use any commercial code for customized applications, it is necessary to develop an interface to implement desired condition. In FLUENT, custom applications are added through a User Defined Function (UDF). Using an UDF gives the ability to solve problems with non-standard conditions. But using an UDF has its own challenges. In the present study, these challenges can be categorized into two groups. The first one emerged in developing a method to treat fluid and solid phases separately and the second one was the implementation of the source terms for mass and energy balance. These terms reaction terms coupled with the heat and mass balance correlations.

Continuum model regard the monolith as a porous medium, with extra terms added to the momentum balance to account for the porous flow resistance. In FLUENT there is an option for porous medium which can be used for this purpose. In this option, permeability in all direction should be defined. For the flow in the axial direction, the permeability can be determined from the pressure drop vs. flow rate data. Because this flow in the channels is laminar, this value can be calculated. There is no radial flow as a result of the structure of the monolith. To prevent radial flow, a radial permeability of for orders of magnitude lower than the axial permeability was used.

Implementing the heterogeneous model in Fluent is more complicated than a homogeneous model. For each phase, solid and fluid, one mass and energy balance should be solved simultaneously. When using a first order reaction, it is not necessary to solve for the solid phase mass balance directly, because the reaction can be written in terms of the fluid concentration, as shown earlier. The solid temperature was introduced by adding the solid phase energy balance as a general differential equation using a User Defined Function.

### **3.4.1 Source terms**

In the UDF, source terms are comprised of heat and mass transfer rates between phases and reaction rate depending on the form of the source term. Depending on the model, the source terms include heat and mass transfer terms, reaction rates, and thermal energy generation terms. Using a source term for reaction rate instead of built-in menu for reaction in Fluent, gives much more ability to define complicated reaction mechanisms.

### **3.4.2 Boundary Conditions**

At the inlet of the converter, for cold flow simulation axial velocity is defined. In these simulations, these velocities correspond to specified mass flow rates which are presented in Table 3.3. When temperature of the inlet gas is changing, the assumption of constant inlet velocity is no longer valid. For these cases, mass flow rate is defined in UDF and inlet velocity will be adjusted by changing temperature. The inlet is far enough from the monolith brick, diffusion across the inlet plane can be neglected and therefore Dirichlet boundary conditions with specified temperature and species concentration can be applied. 5% turbulence intensity is assumed for  $\kappa$  and  $\epsilon$  calculations. For the reactor outlet, outflow boundary condition with backflow with constant temperature is used.

For outside surface of the reactor, convection boundary condition for temperature condition is applied. For each case, heat transfer coefficient and surrounding temperature defined correspondingly and for mass conservation purposes, zero flux condition was imposed.

For heterogeneous model, wall condition with zero flux between monolith and insulation wall is applied. However, heat transfer between fluid and solid phase of the monolith still remains in this boundary for heterogeneous model. In that

boundary, there is contact between fluid and solid phases of the monolith and solid wall and the real condition of the boundary is complicated and cannot be determined in a continuum model. In Table 3.4, typical values of some of the above mentioned parameters are given.

Table 3.4- Typical values for some of important parameters at 450 K

Parameter	400-STD CPSI	900 CPSI	400-thin CPSI	dimension	Description
$D_H$	0.001	0.000726 4	0.001206 5	meter (m)	Hydraulic diameter
$A_v$	2480	4052.863 436	2594.280 978	1/m	surface to volume ratio
$P$	1.01E+05	1.01E+05	1.01E+05	Pa	Pressure
$\tau$	0.5	0.5	0.5	None	tortuosity
$\epsilon_w$	0.12	0.12	0.12	None	washcoat porosity
$\epsilon_m$	0.62	0.736	0.7825	None	monolith porosity
$d_p$	1.00E-08	1.00E-08	1.00E-08	meter (m)	pore diameter
$L_c$	4.80E-05	2.95E-05	4.30E-05	meter (m)	characteristic length
$A_0$	7.000E+1 5	7.000E+1 5	7.000E+1 5	1/s	pre-exponential factor
$R_g$	8.314	8.314	8.314	J/mol.K	gas constant
$E$	1.007E+0 5	1.007E+0 5	1.007E+0 5	J/mol	activation energy
$M_{w,CO}$	28	28	28	g/mol	CO molecular weight
$Nu, Sh$	4	4	4	None	Nusslet and Sherwood numbers
$T_s$	450	450	450	K	Surface temperature
$T_f$	450	450	450	K	Fluid temperature
$K_r$	1.413E+0 4	1.413E+0 4	1.413E+0 4	1/s	Rate constant
$D_{eff}$	1.95E-06	1.95E-06	1.95E-06	m <sup>2</sup> /s	Effective diffusivity
$\phi$	4.09E+00	2.51E+00	3.66E+00	None	Thiele modulus
$\eta$	2.44E-01	3.93E-01	2.73E-01	None	Effectiveness factor
$D_{ab}$	4.02E-05	4.02E-05	4.02E-05	m <sup>2</sup> /s	Binary diffusion Coefficient (CO in air)
$K_m$	1.61E-01	2.22E-01	1.33E-01	m/s	Mass transfer coefficient
$K_{app}$	2.03E+02	3.82E+02	1.98E+02	1/s	Apparent rate constant
$Y_{CO}$	1.00E-03	1.00E-03	1.00E-03	None	Co mole fraction @ inlet
$C_{tot}$	2.71E+01	2.71E+01	2.71E+01	mol/m <sup>3</sup>	Total concentration
$R$	5.50E+00	1.04E+01	5.36E+00	mol/m <sup>3</sup> . s	Rate of the reaction

# Chapter 4

## Simulation results and discussion

The results of the study are given in three different parts. In the first part, only isothermal flow without reaction is considered. In these runs the converter is at a temperature of 300 K, as are the surroundings. In the second part, a comparison is made as the converters are heated without any chemical reaction occurring. In this part, the temperature of the inlet gas is ramped from 300 K to 700 K. In the third and final part, both heat transfer and reaction are present. In this part, CO conversion is studied and comparison between different cases is made.

### 4.1 Cold flow results

In the first part of the investigation, isothermal flow was studied under steady state. No heat transfer and reaction are present. The main goal of this part was to study the hydrodynamics of different geometries. Velocity, pressure, and turbulent kinetic energy profiles of each case were compared. Three different sizes (short, middle and long), three different velocities corresponding to different mass flow rates mentioned in Table 3.3 (7.6, 15.11 and 30.22 m/s) and three different cell configuration (400-std, 900 and 400-thin CPSI) were considered at an inlet temperature of 300 K. These simulations gave useful data on velocity, pressure and turbulent kinetic energy profile throughout the converter which help us to decide on the optimum hydrodynamic condition of the converter. The results are presented in four different sections in detail. In the last section, the effect of inlet cone length on the aforementioned parameters has also been discussed. With these results, we can have a better understanding of the main parameters involved

in converter design and then can introduce heat transfer and reaction in the monolith.

#### 4.1.1 Pressure profiles in the monolith

Pressure drop is one of the main concerns in converter design. High pressure drops in monolithic section affect performance of the converter drastically and is always tried to be avoided. As it is illustrated below, pressure profiles for all inlet velocity values are almost the same. High pressure regions occur near the center of the converter. Below is the result for the mid-length converter. The trend is the same for short and long-length converters.

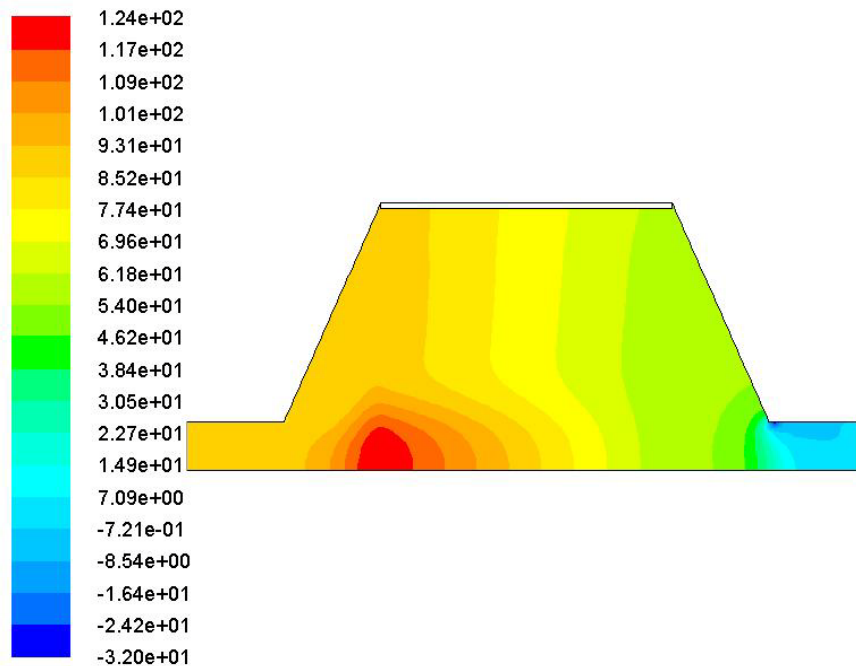


Figure 4.1 - Pressure contours for cold flow through 400 CPSI std wall monolith at an inlet velocity of 7.6 m/s. The medium length converter is shown

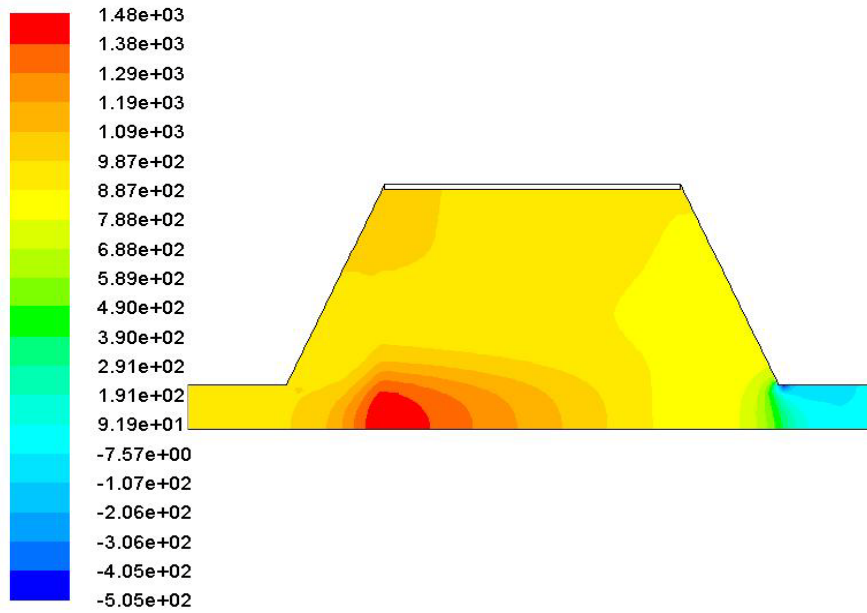


Figure 4.2 - Pressure contours for cold flow through 400 CPSI std wall monolith at an inlet velocity of 15.11 m/s. The medium length converter is shown

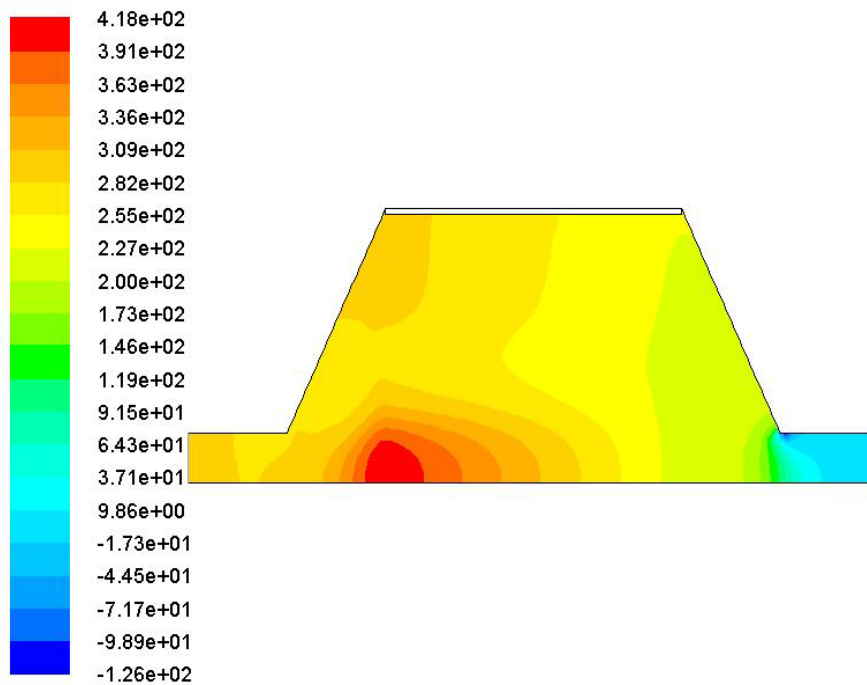


Figure 4.3 - Pressure contours for cold flow through 400 CPSI std wall monolith at an inlet velocity of 30.22 m/s. The medium length converter is shown

However, with increasing the velocity, pressure drop increases in the monolith brick. In Figure 4.4, pressure drop of monolith brick for different velocities has been shown. Pressure drop for respective radial positions of the inlet and outlet of the monolith brick has been calculated. For the lowest velocity, pressure drop with radial position in the converter is almost uniform. But with increasing velocity, high pressure regions occur in the converter near the axis which causes more pressure drop in the system.

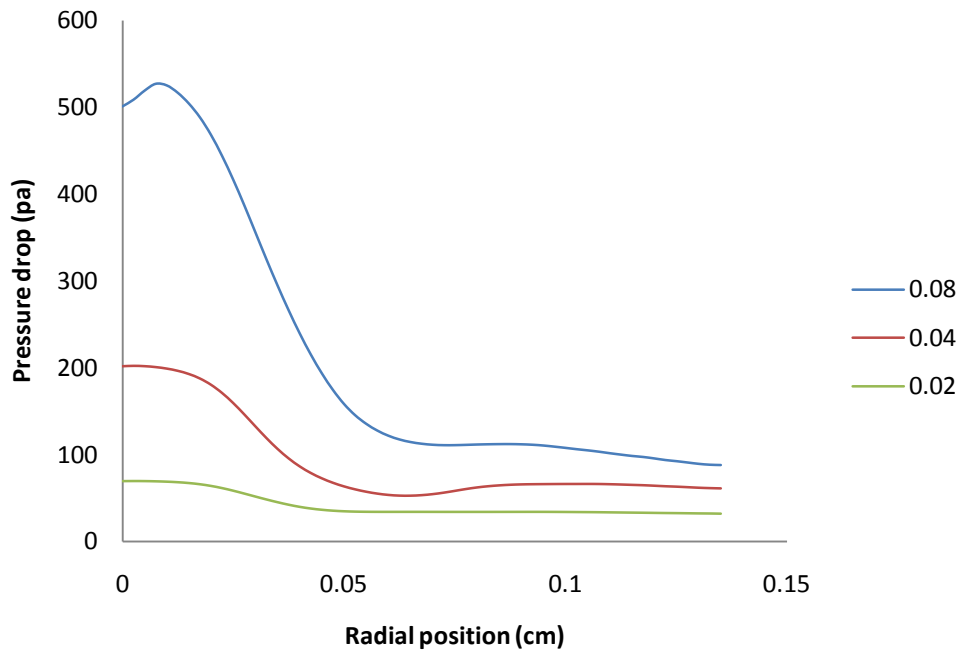


Figure 4.4- Pressure drop of the monolith brick with respect to radial position. Velocity is changing from 0.02 kg/s (7.6 m/s) to 0.08 kg/s (30.22 m/s). Medium length converter is regarded.

The effect of the cell density on the pressure profile through the converter is the other variable that can be discussed. It is shown that the configuration with 400-thin CPSI has the most uniform profile. On the other hand, pressure loss is the lowest for 400-thin CPSI. Below is the result for the effect related to cell numbers. Here the velocity and geometry size are 15.11 m/s and long model respectively and cell numbers are as a variable.

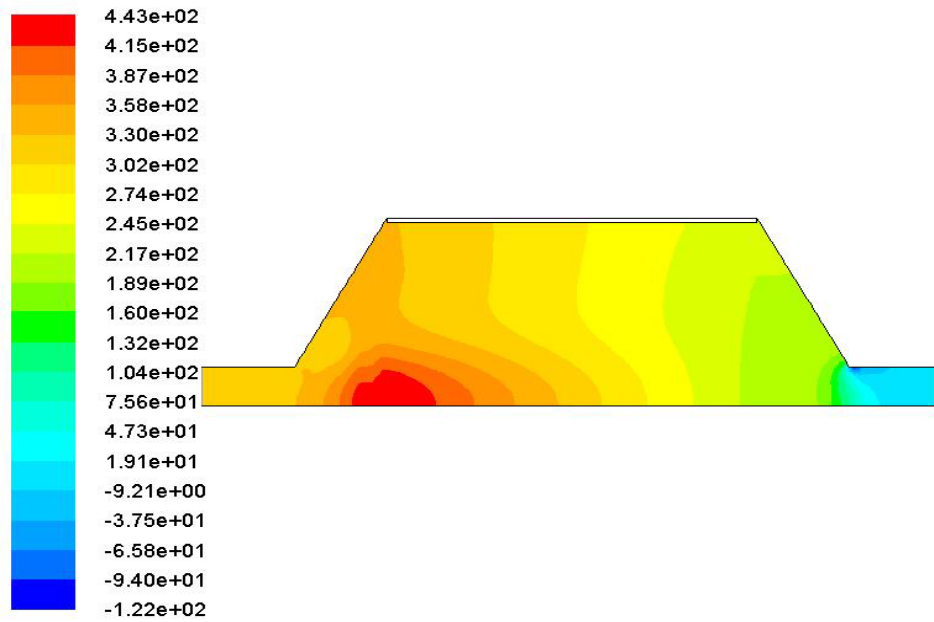


Figure 4.5 - Pressure contours for cold flow through 400 CPSI std wall monolith at an inlet velocity of 15.11 m/s. The medium length converter is shown

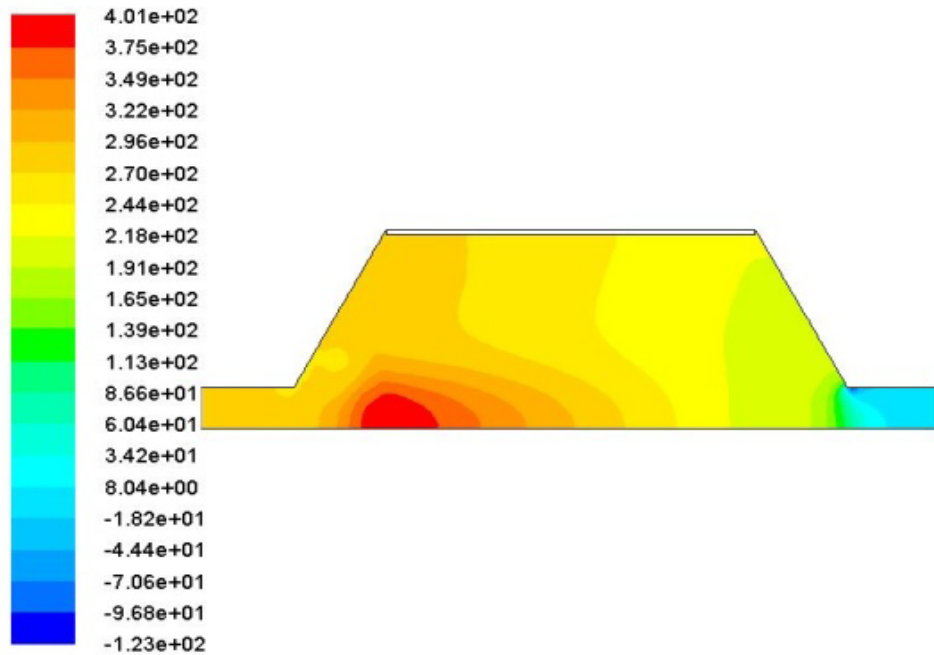


Figure 4.6 - Pressure contours for cold flow through 400 CPSI thin wall monolith at an inlet velocity of 15.11 m/s. The medium length converter is shown

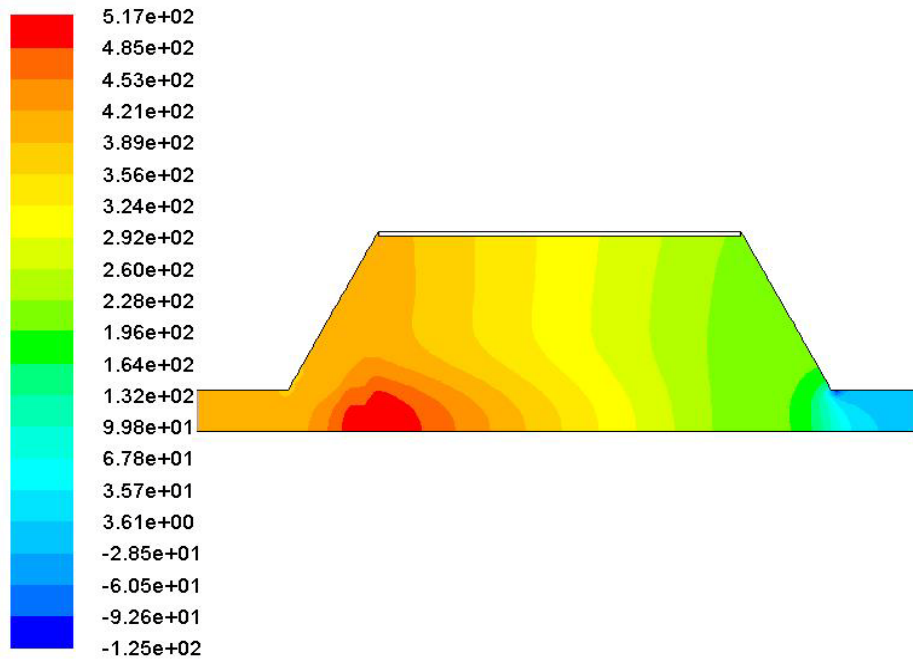


Figure 4.7 - Pressure contours for cold flow through 900 CPSI wall monolith at an inlet velocity of 15.11 m/s. The medium length converter is shown

In Figure 4.7, pressure drop of the monolith brick for different monolith CPSI configurations is presented. As discussed above, 400-thin is the best configuration with respect to pressure drop concerns. It is due to the fact that 400-thin has the biggest channel diameter among the other with means less pressure drop.

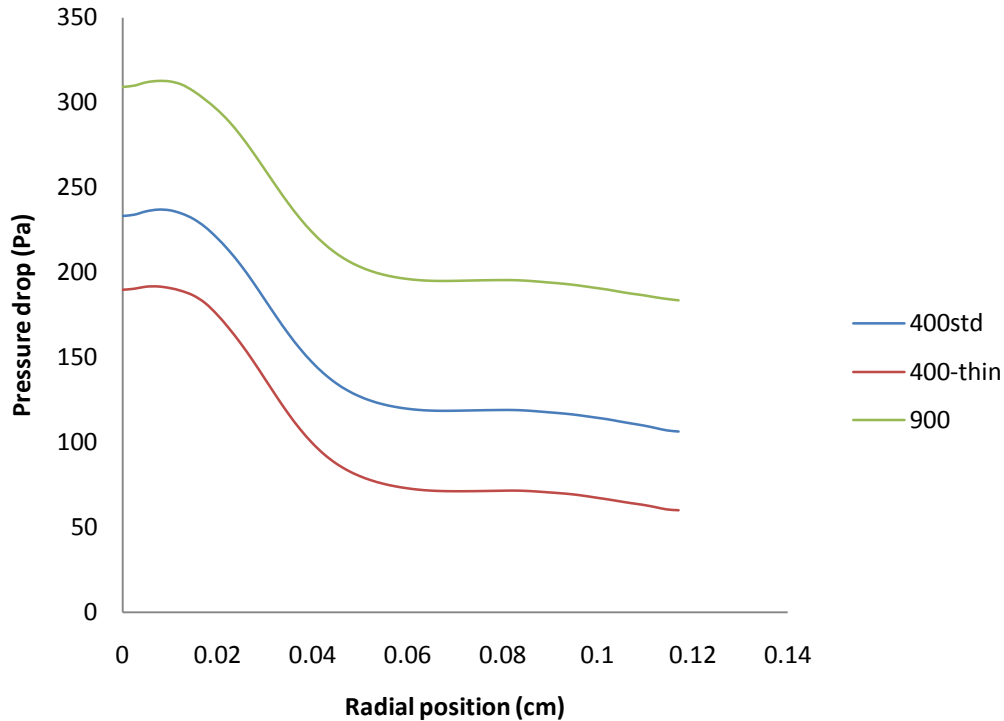


Figure 4.7- Pressure drop of the monolith brick with respect to radial position for different monolith CPSI is the. Long length converter is regarded and inlet velocity is 15.11 m/s.

And for the last comparison, we changed the geometry while other parameters were constant. To do so, we choose inlet velocity as 15.11 m/s and CPSI to be 400std. The effect of the geometry on pressure profile is presented in Figure 4.8. Long geometry has the biggest pressure drop which is resulted from the fact that it has the biggest monolith length. There is an interesting fact about the pressure drop profile for middle geometry. As you can see pressure drop is not completely decreasing with radial position in monolith and at around  $r=6$  cm it begins to increase. This behavior is resulted from circulation patterns in the converter which will be discussed in the following sections.

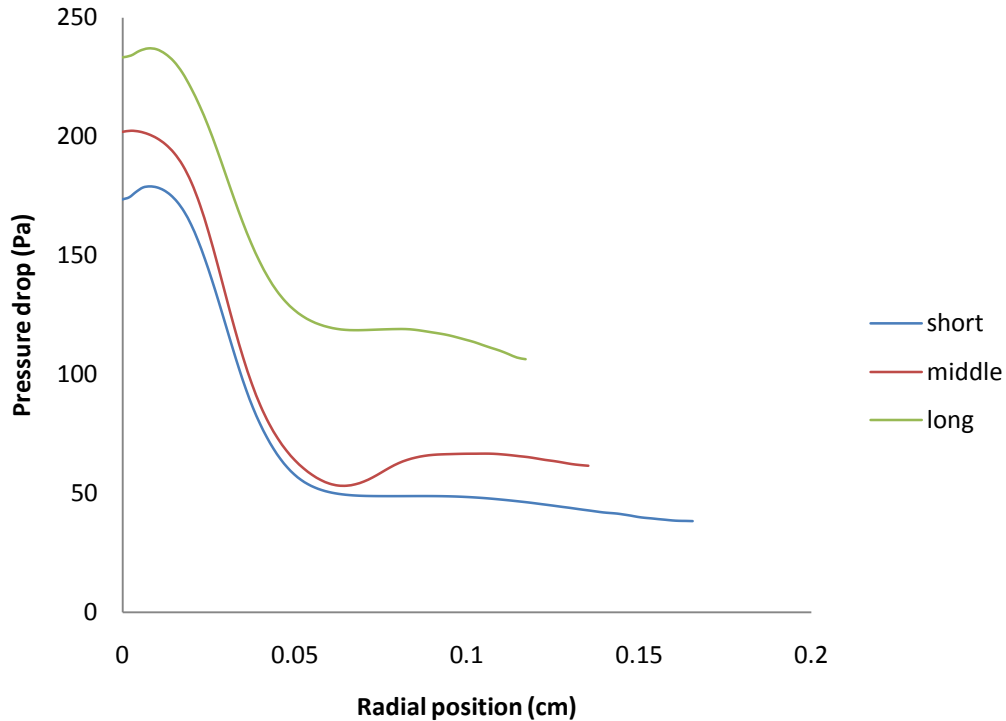


Figure 4.8- Pressure drop of the monolith brick in the monolith with respect to radial position. Inlet velocity is 15.11 m/s and monolith CPSI is 400 std. short, middle and long size converters is regarded.

#### 4.1.2 Velocity profiles in the monolith

Both geometry size of the converter and monolith CPSI change the velocity profile throughout the converter. The most desirable profile for velocity in the converter is uniform profile. In uniform profile, velocity does not change in radial direction and therefore all sections of the monolith brick have the same hydrodynamics. First we examine the effect of the geometry size on the velocity at monolith entrance while monolith CPSI and converter inlet velocity are constant. The results are shown in Figure 4.9. As you can see, the axial velocity profile of the long model is more uniform at the monolith entrance, which implies a better circulation pattern for long model. Lack of a proper circulation has lead to very low axial velocity for short model both at near the axis and near the walls of

the converter. While the long model has a higher average velocity at the entrance of the monolith, middle geometry has the highest velocity near the axis. This interesting result is originated from circulation patterns and eddy formation near the entrance of the monolith. In the next section this issue is fully discussed.

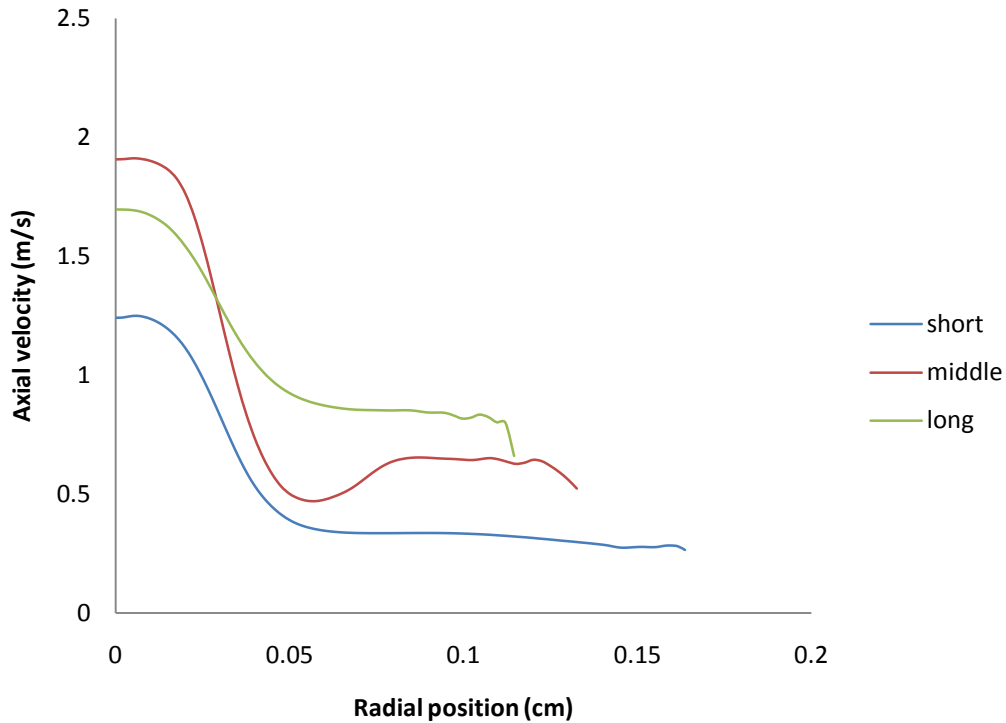


Figure 4.9 -Axial velocity at the monolith entrance with respect to radial position. Short, middle and long converters are compared. Inlet velocity is 15.11 m/s and monolith CPSI is 400 std.

The effect of monolith CPSI on the velocity at the monolith brick entrance is the other parameter that could be discussed. In this case inlet velocity in 30.22 m/s and middle size model has been chosen. As it is presented in Figure 4.10, 400-thin and 900 CPSI configurations has almost the same profile and velocity magnitude at the monolith entrance, while 400 CPSI has significantly lower axial velocity near the axis.

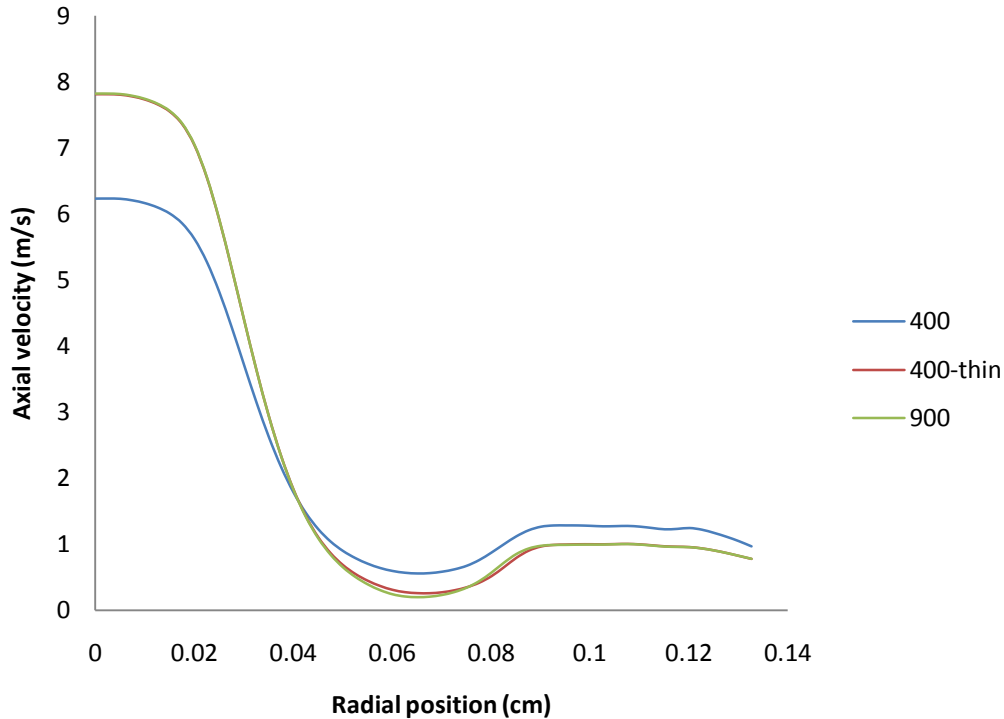


Figure 4.10 -Axial velocity at the monolith brick entrance with respect to radial position. Different monolith CPSI configurations are compared. Inlet velocity is 30.22 m/s and middle size model is shown.

### 4.1.3 Turbulent kinetic energy profiles in the monolith

Generation of eddies is an important parameter which should be concerned in converter design. We can locate eddies in the system through measuring Turbulent kinetic energy ( $k$ ), so that in the places which  $k$  is significantly higher, eddies occur.

In overall, with increasing of the inlet velocity, eddies occur at higher distances from axis. This trend can be seen for all geometry sizes and different monolith CPSI. In Figure 4.11 to 4.13, the results for long size model with 400-thin CPSI are presented.

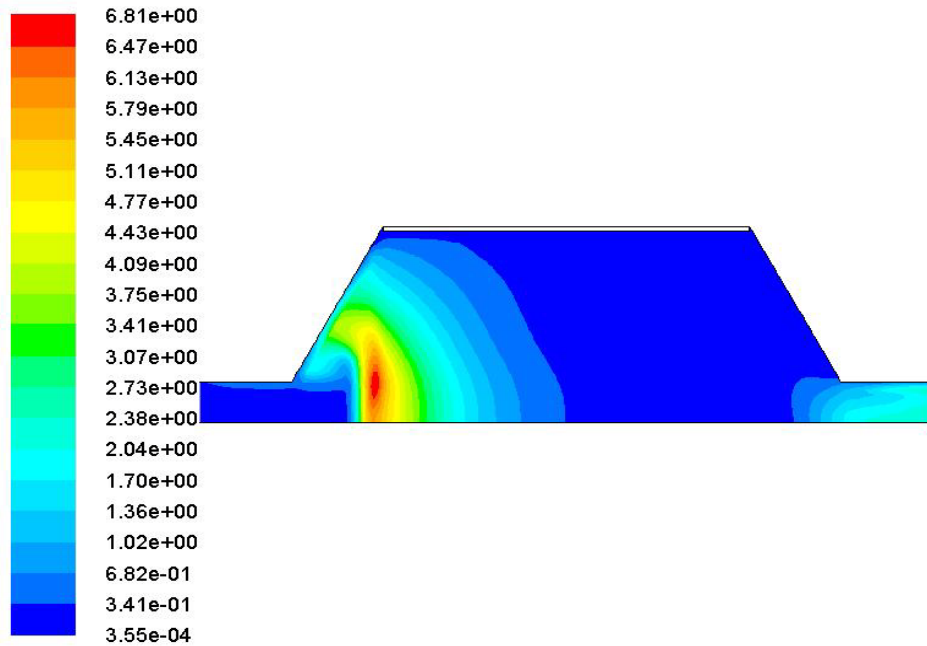


Figure 4.11 – Turbulent kinetic energy contours for cold flow through 400 CPSI thin wall monolith at an inlet velocity of 7.6 m/s. The long length converter is shown

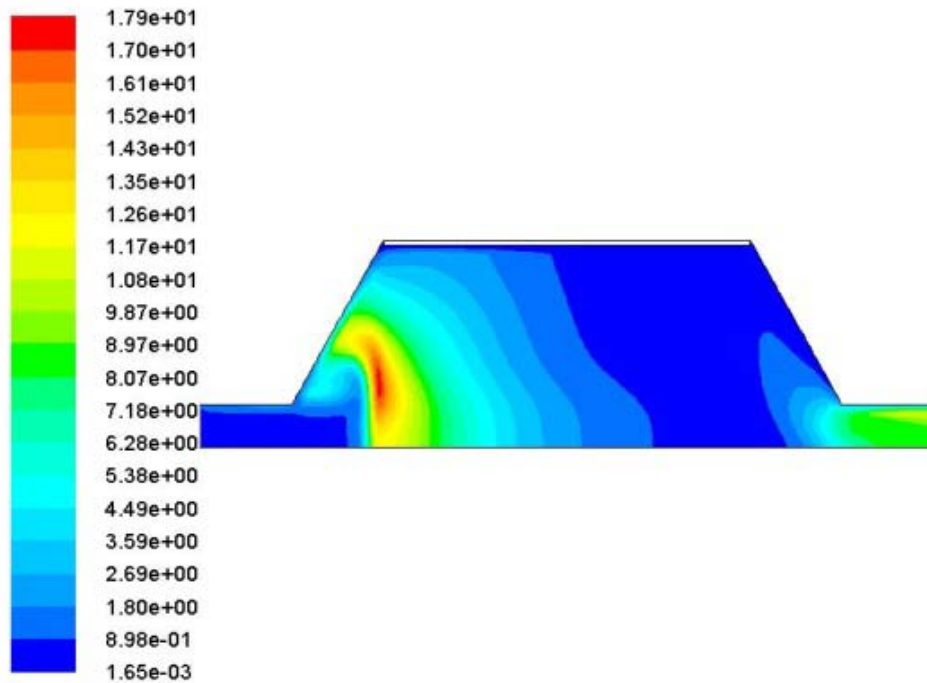


Figure 4.12 – Turbulent kinetic energy contours for cold flow through 400 CPSI thin wall monolith at an inlet velocity of 15.11 m/s. The long length converter is shown

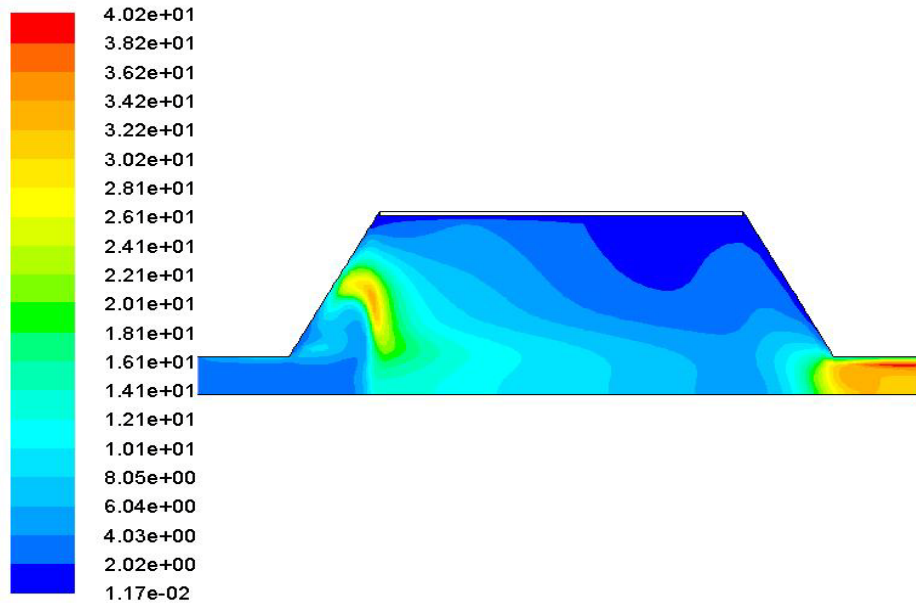


Figure 4.13 – Turbulent kinetic energy contours for cold flow through 400 CPSI thin wall monolith at an inlet velocity of 30.22 m/s. The long length converter is shown

It is interesting to note that with respect to different geometry sizes, the middle model has the lowest turbulence present in the converter. This fact is shown in Figures 4.14 to 4.16. Also, in this geometry, eddies occur at the places with higher distance from axis. The results for different geometries are presented below. This behavior explains the results for axial velocity and pressure profiles for middle geometry. In the middle case, near the axis there is no eddies and circular flow; therefore axial velocity of the middle size converter is the highest amongst the other geometries.

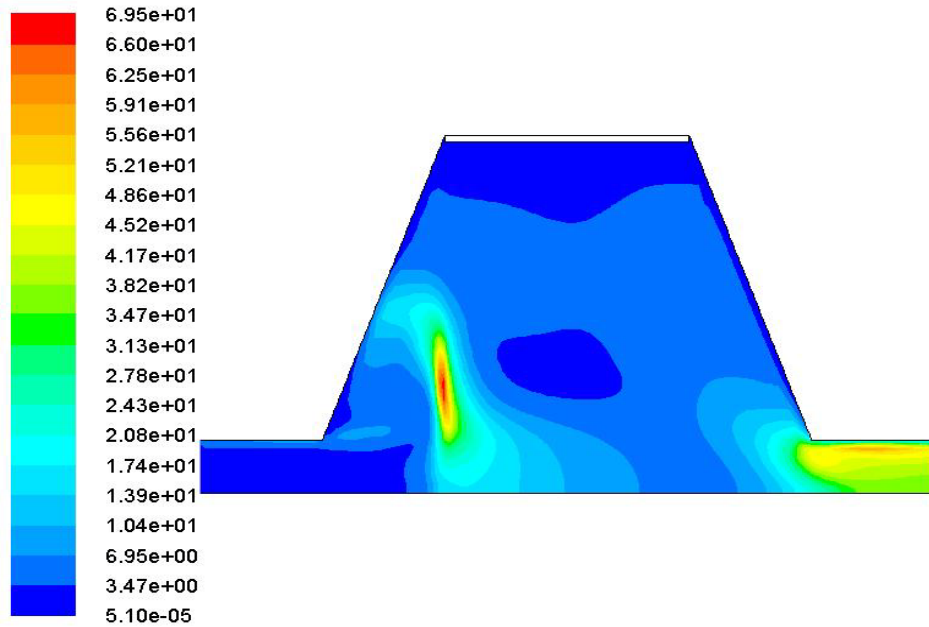


Figure 4.14 – Turbulent kinetic energy contours for cold flow through 400 CPSI monolith at an inlet velocity of 30.22 m/s. The short length converter is shown

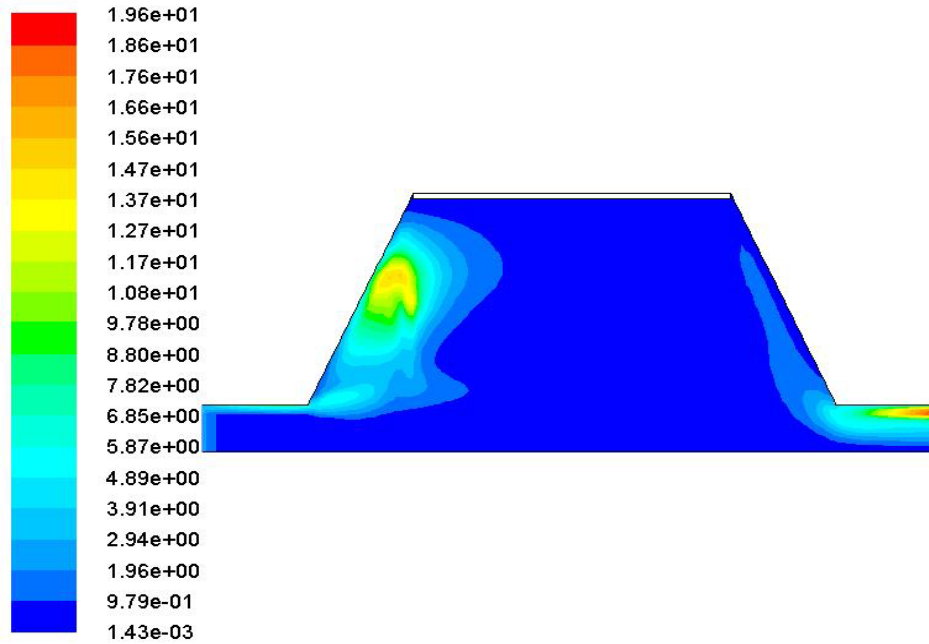


Figure 4.15 – Turbulent kinetic energy contours for cold flow through 400 CPSI monolith at an inlet velocity of 30.22 m/s. The middle length converter is shown

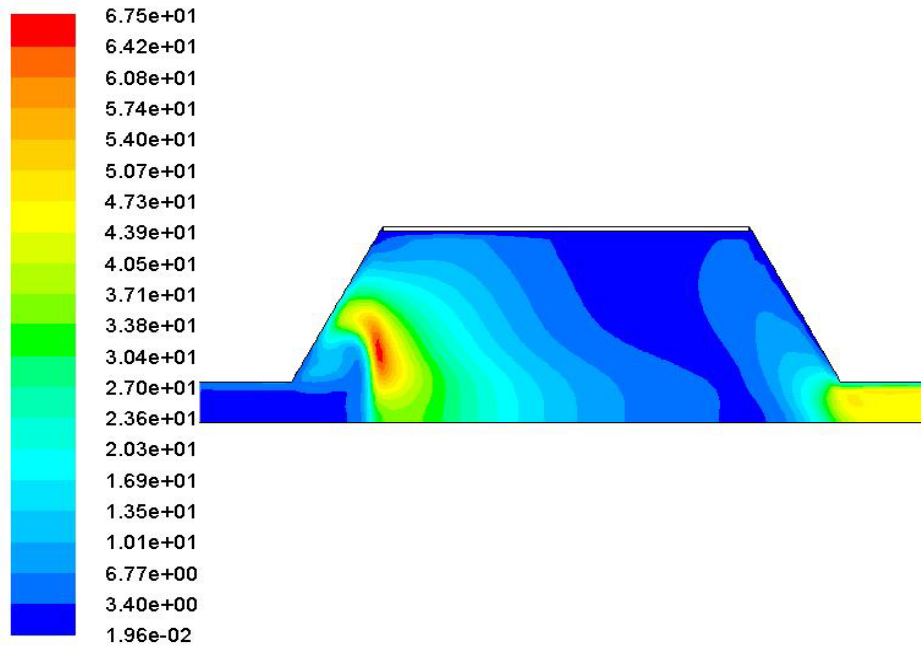


Figure 4.16 – Turbulent kinetic energy contours for cold flow through 400 CPSI monolith at an inlet velocity of 30.22 m/s. The long length converter is shown

The effect of CPSI on turbulent kinetic energy profiles is not significant. In overall, CPSI has little effect on the location of eddies, however 400-thin CPSI has the lowest turbulent kinetic energy,  $k$ , among other configurations.

#### 4.1.4 Effect of inlet cone length on hydrodynamics of the converter

In this part, the effect of inlet cone length on different parameters, pressure, velocity and turbulent kinetic energy, has been discussed. We chose middle size model as the basis and then increased the length of inlet cone from 5cm to 10 cm to investigate the pressure, velocity and turbulence kinetic energy distribution in the converter. In this part, inlet velocity is constant at 15.11 m/s and monolith brick with 400 CPSI has been regarded.

As shown in Figure 4.17, axial velocity is decreasing with the extension of the inlet cone and uniformity of the flow at the entrance of the monolith increases.

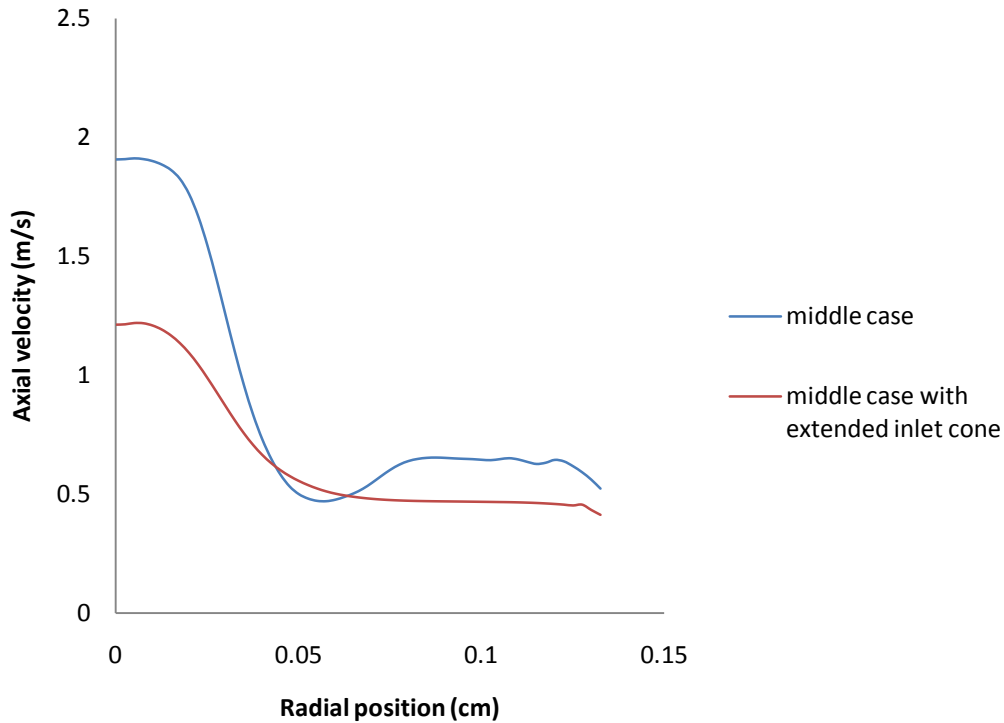


Figure 4.17- Axial velocity at the entrance of the monolith brick. Middle size model was chosen as the basis and inlet cone extended to 10 cm. monolith CPSI is 400 std and inlet velocity is 15.11 m/s.

If we take a look at the places which eddies occur in each system, we can understand the cause of higher velocity near the axis for middle size geometry. As shown in Figure 4.18 and 4.19, in the extended inlet cone model eddies occur near the axis, resulting in circulating flow and lower axial velocity in that region.

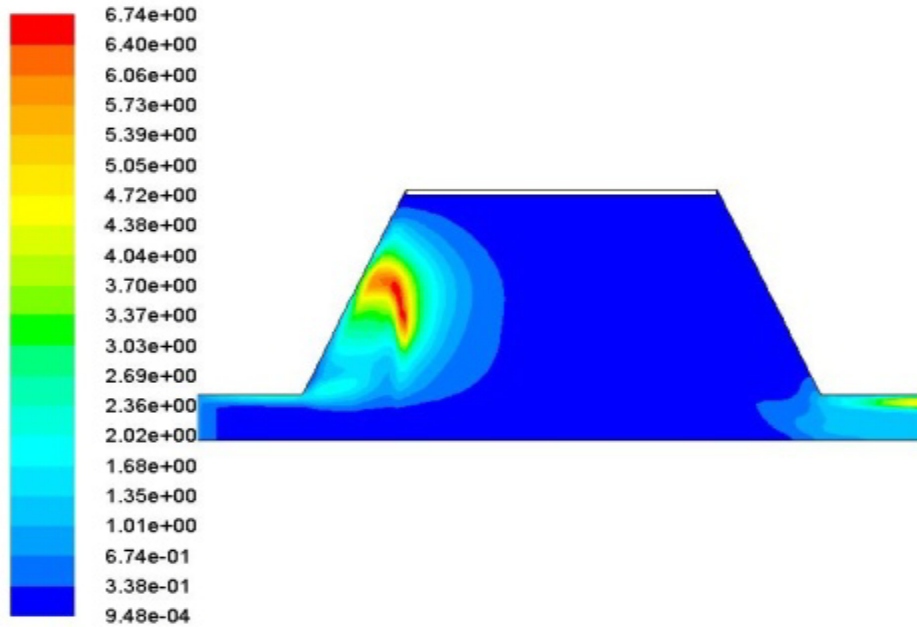


Figure 4.18 – Turbulent kinetic energy contours for cold flow through 400 CPSI monolith at an inlet velocity of 15.11 m/s. The middle length converter is shown

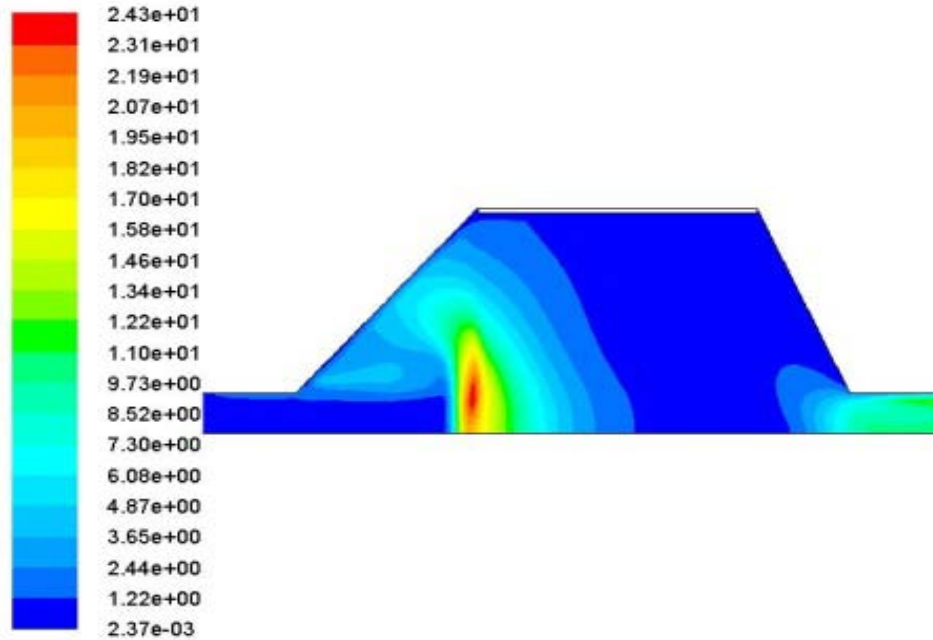


Figure 4.19 – Turbulent kinetic energy contours for cold flow through 400 CPSI monolith at an inlet velocity of 15.11 m/s. The middle length converter with extended inlet cone is shown

By measuring pressure drop for the two cases, it is shown that extended model has a lower pressure drop in monolith brick with respect to normal middle length geometry. This fact is shown in figure 4.20.

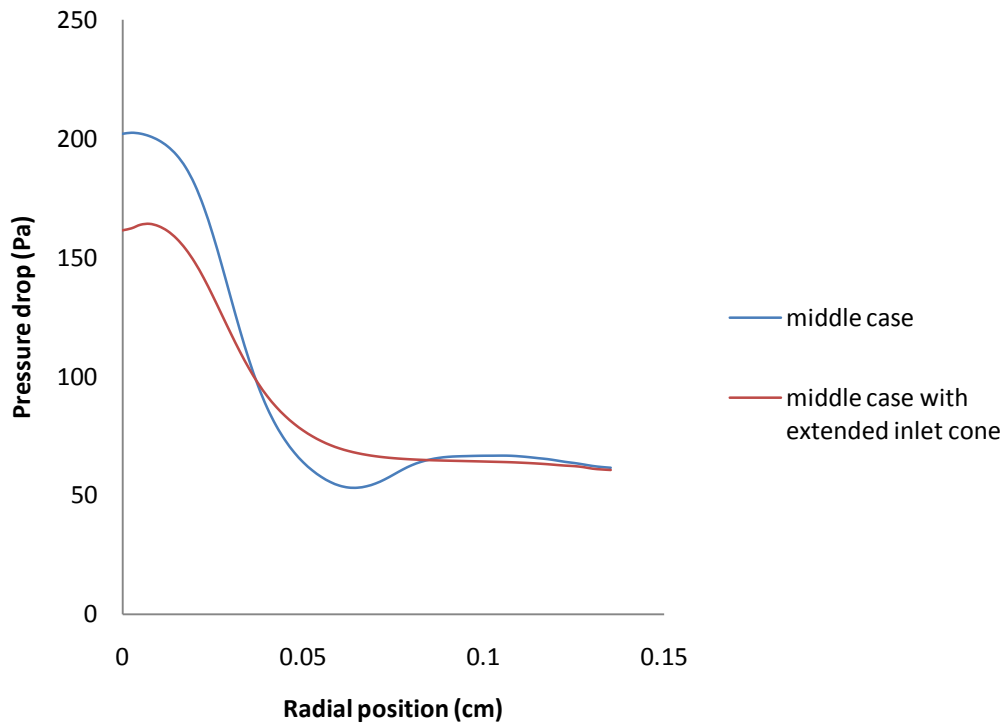


Figure 4.20- Pressure drop of monolith brick with respect to radial position. Middle size geometry and middle size with extended inlet cone are compared. Inlet velocity is 15.11 m/s and monolith CPSI is 400 std.

## **4.2 Temperature effect in catalytic converter, heterogeneous model**

In this part of the study, we investigated the effect of the temperature on catalytic converter based on heterogeneous model implemented in monolithic brick of the converter. In this part, no reaction occurs in the converter. In order to do so, we used an UDF for implementing the heterogeneous model throughout the monolith, so we could investigate solid and fluid properties separately. The main goal of this part is to determine temperature profile for different cases and the effect of involved parameters on temperature distribution in converter.

For the first part of these simulations, middle size geometry is investigated on different CPSI; then the effect of different geometries, i.e. short, middle and long is discussed. Also in all simulation inlet mass flow rate was chosen to be 0.02 kg/s,  $h_{out}$  is 10 w/ m<sup>2</sup>.k, and inlet temperature ramp is 20°C /S. Temperature is increasing linearly from 300 k to 700 in 20 seconds and then remains constant at 700.

### **4.2.1 The effect of CPSI:**

In this part, we studied temperature profile in the converter 100 seconds after introducing to ramping temperature. It should be mentioned that after 20 seconds, inlet temperature reaches 700 degrees and after that, inlet temperature remains constant.

Based on the results shown in Figure (4.21) to (4.23) for middle size geometry, 400-thin CPSI warmed up more quickly than other CPSI configurations.

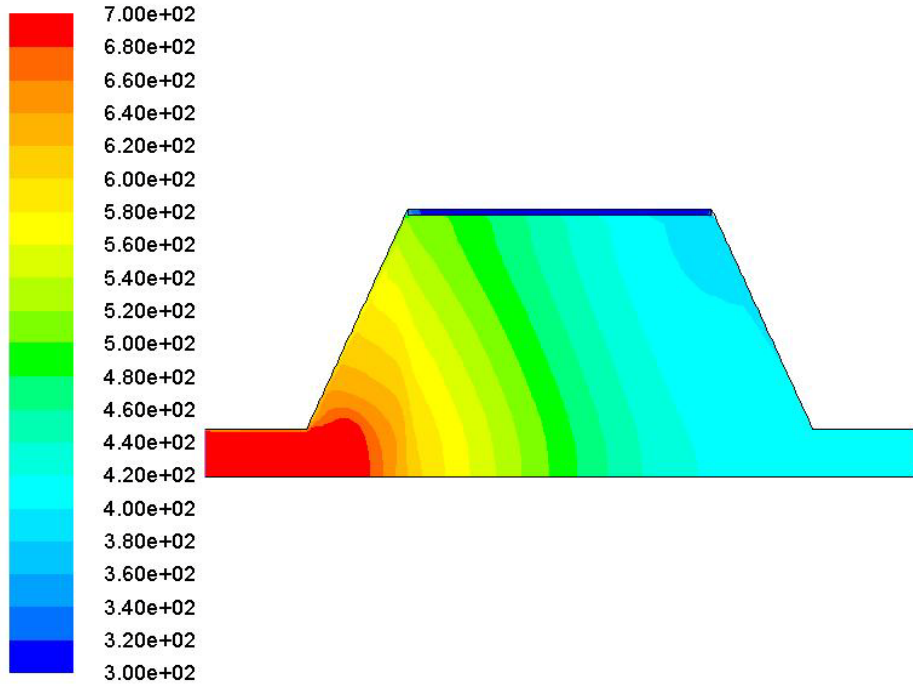


Figure 4.21 – Temperature contours through 400 CPSI monolith at an inlet mass flow rate of 0.02 Kg/s. The middle length converter is shown

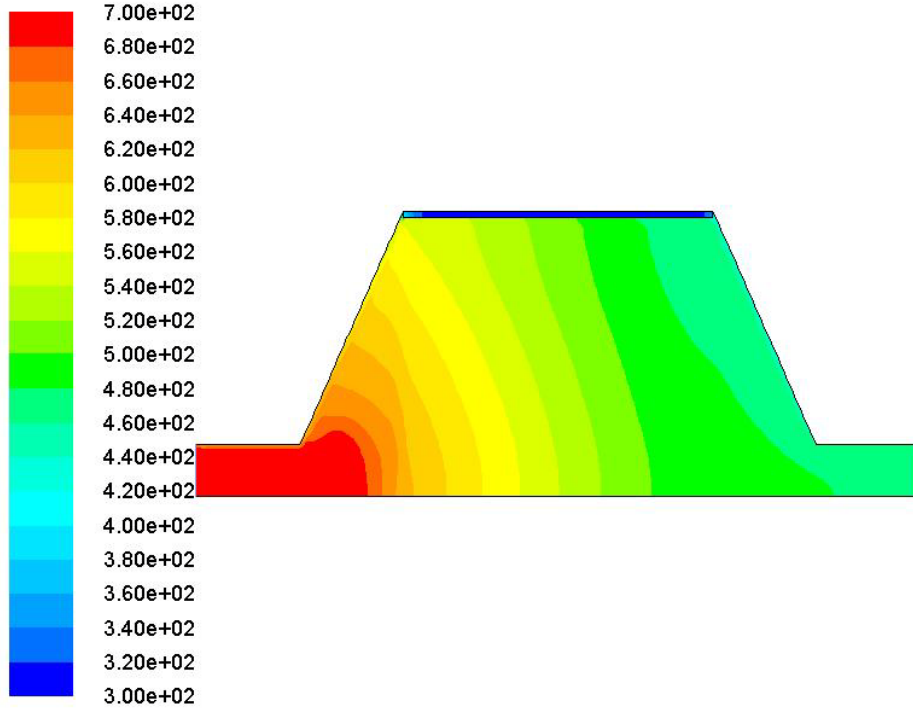


Figure 4.22 – Temperature contours through 900 CPSI monolith at an inlet mass flow rate of 0.02 Kg/s. The middle length converter is shown

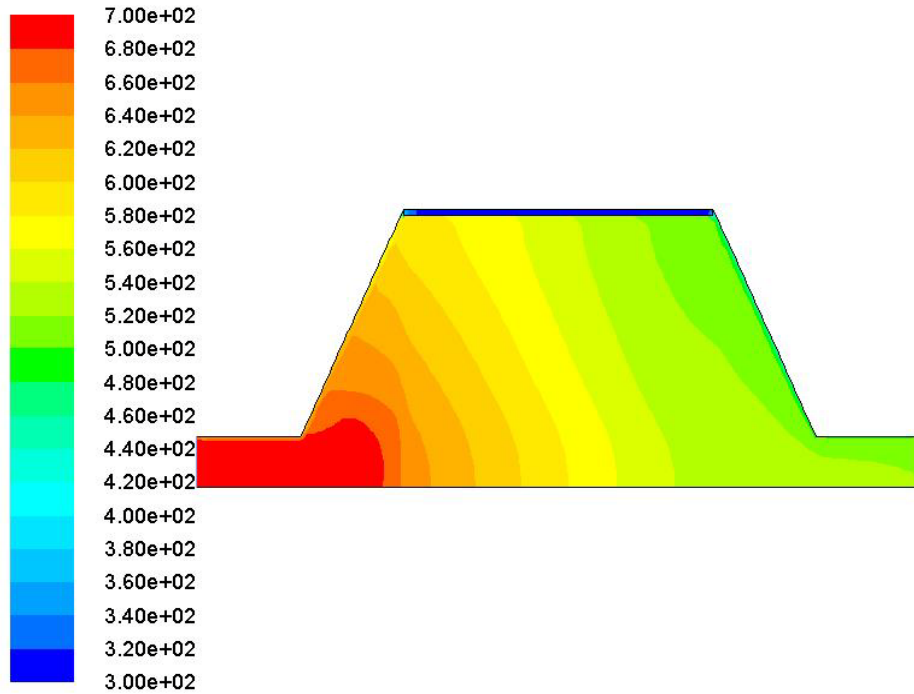


Figure 4.23 – Temperature contours through 400 CPSI thin wall monolith at an inlet mass flow rate of 0.02 Kg/s. The middle length converter is shown

In Figure 4.24, these results are illustrated in terms of average temperature of solid in monolith brick. Again, we can see that 400-thin CPSI configuration warms up more quickly than other configurations. Note that velocity in the channels is almost the same for 400-thin and 900 CPSI configurations, but 400-thin CPSI has less bulk density ( $306 \text{ Kg/m}^3$ ) than 900 CPSI ( $389 \text{ Kg/m}^3$ ), resulting in warming up more quickly. 400 CPSI has both the lowest velocity in the channels and highest bulk density ( $596 \text{ Kg/m}^3$ ), therefore it warms up more slowly than others.

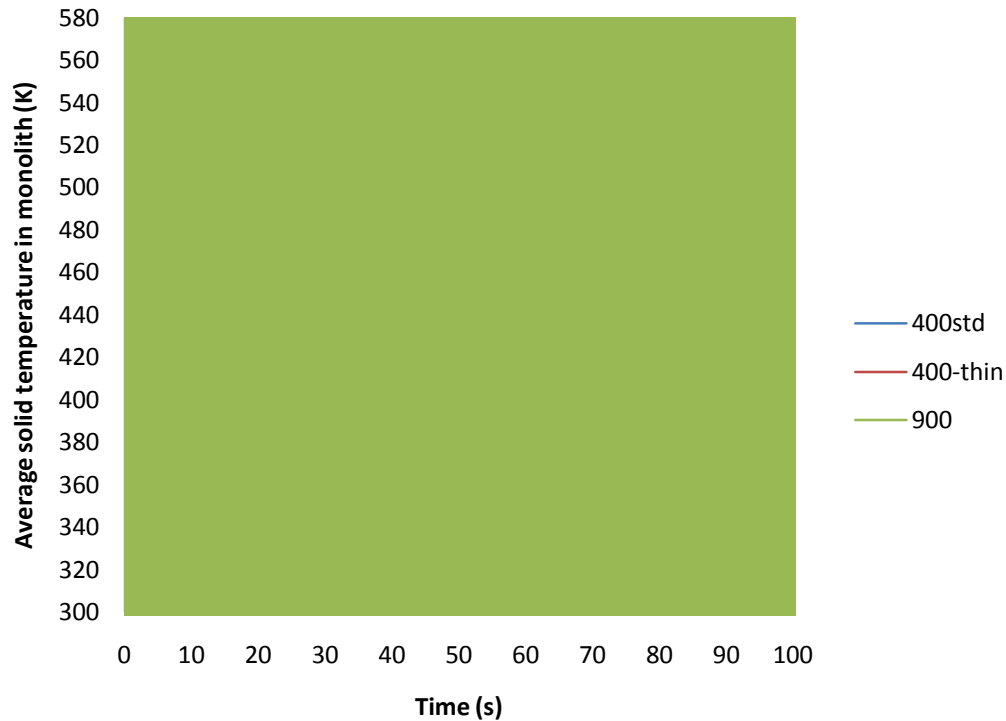


Figure 4.24- Average solid temperature of the monolith brick with time for a feed with 0.02 Kg/s mass flow rate. Different monolith CPSI configurations are compared. Middle size converter is shown

Another important parameter is the heat transfer between fluid and solid in monolith brick. Bulk density of the monolith brick is the main parameters in this regard. In Figures 4.25 to 4.27, results for different CPSI configurations are shown. For 400-thin CPSI model, there is almost no difference between solid and fluid temperature, i.e. it is completely isothermal in the monolith brick. As discussed before, 400-thin CPSI has the lowest bulk density, i.e. thermal mass of monolith brick, resulting in sooner heating up. But with increasing the bulk density for 900 CPSI and 400 CPSI configurations, this isothermal behavior of solid and fluid diminishes and the highest temperature difference occurs for 400 CPSI model. Channel diameter and contact time are other parameters involved in heat transfer between solid and fluid in monolith brick; however as far as channel

diameter difference is not significant for these configuration, and velocity in the channels is close to each other for these models, their effect is not seen here.

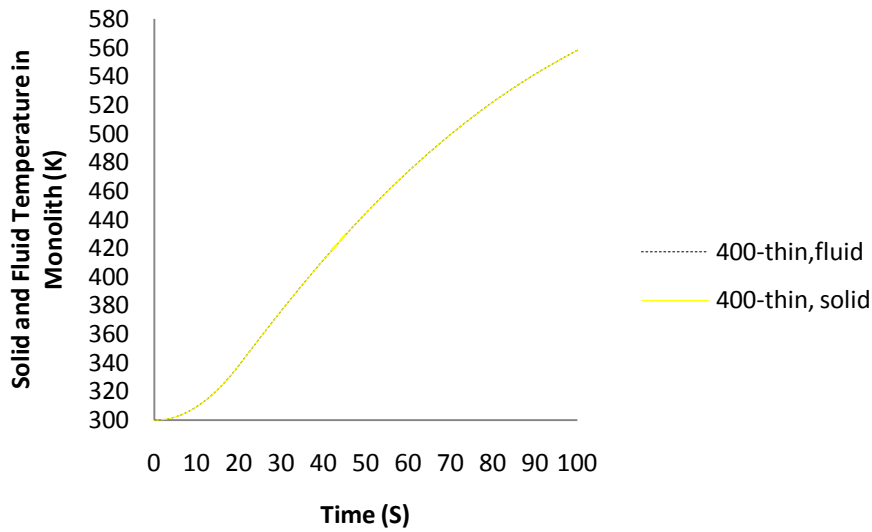


Figure 4.25- Average solid and fluid temperatures in the 400 CPSI with thin wall monolith brick with time for a feed with 0.02 Kg/s mass flow rate are shown. Middle size converter is shown

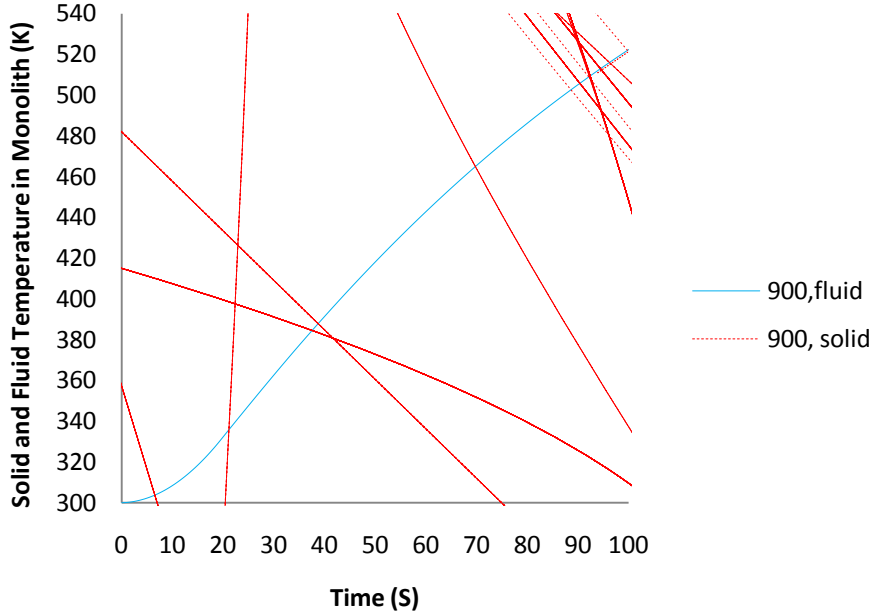


Figure 4.26- Average solid and fluid temperatures in the 900 CPSI monolith brick with time for a feed with 0.02 Kg/s mass flow rate are shown. Middle size converter is shown

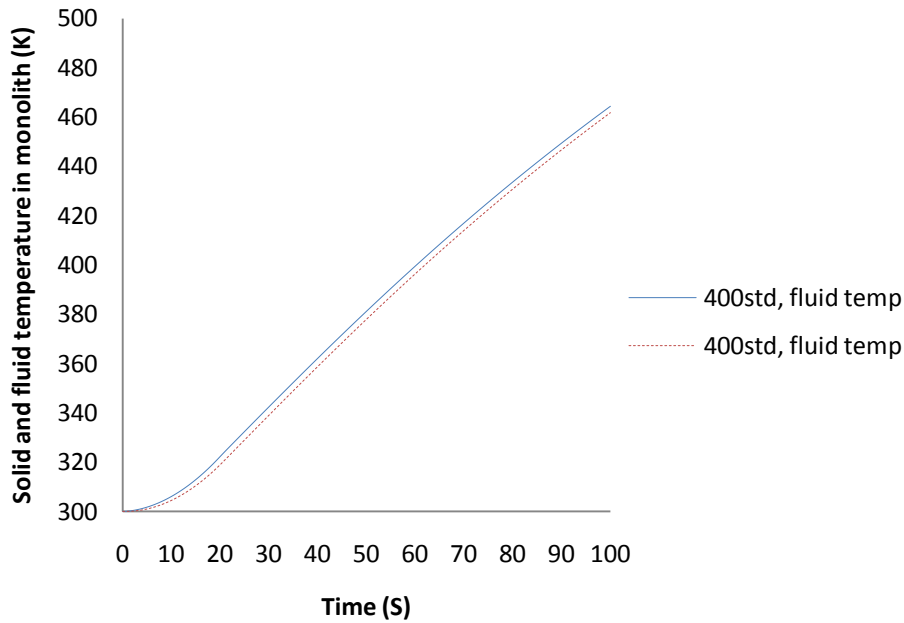


Figure 4.27- Average solid and fluid temperatures in the 400 std CPSI monolith brick with time for a feed with 0.02 Kg/s mass flow rate are shown. Middle size converter is shown

#### 4.2.2 The effect of size on temperature profile:

In this section, 400 CPSI monolith brick was chosen as the basis and the simulation for different converter sizes was performed. The results are shown in Figure 4.28. Long size converter has the highest average temperature of the monolith brick after 100 s. This behavior is anticipated based on the fact that long geometry has the highest velocity in the channels and therefore sooner warming up of the converter. In short size geometry, some part of the converter, mostly the regions with higher distance from the axis, the velocity in channels is very low due to improper flow circulation. This fact makes short size geometry to have the lowest average temperature which means late warming up. As it is shown, in the first 30 seconds after the start, all sizes have the same warming profile but after

that, circulation patterns begin to show their effect and temperature profiles start to diverge.

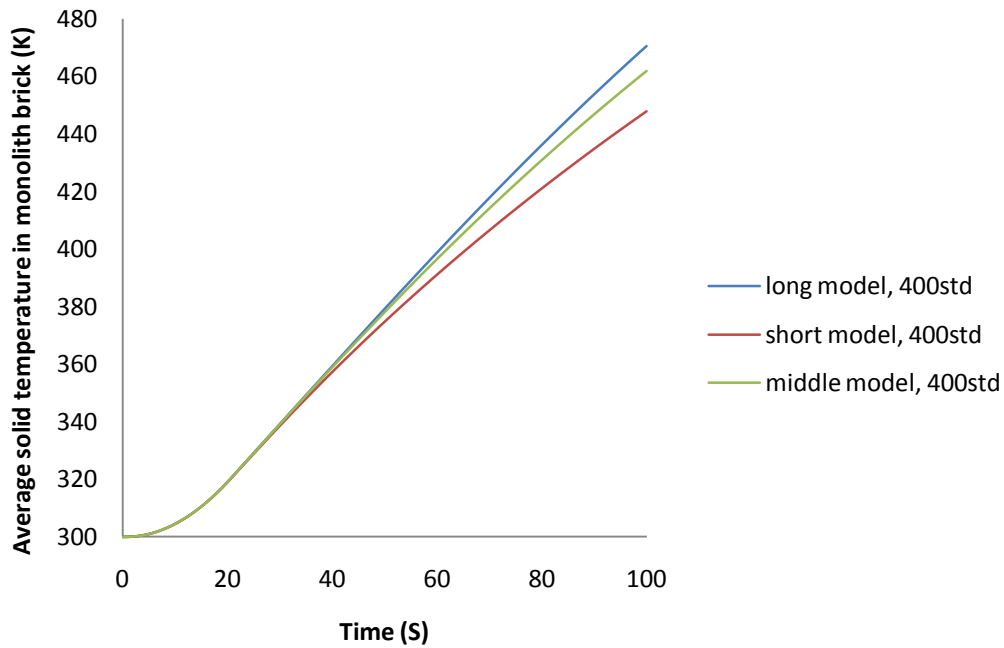


Figure 4.28- Average solid temperature of the monolith brick with time for a feed with 0.02 Kg/s mass flow rate. Short, middle and long length converters are compared. Monolith brick CPSI is 400 std.

Changing the size of the converter did not affect solid and fluid temperature difference in the monolith brick however. In Figure 4.29, this behavior is shown. Both short and long geometries showed the same temperature difference between solid and fluid. This fact implies again that velocity in the channels, which is significantly different for short and long geometries and therefore contact time of the fluid and solid, do not have a considerable effect on heating behavior of the solid by fluid. As discussed in the last section, thermal mass of the monolith brick is the main parameter which is remained constant ( $596 \text{ kg/m}^3$  for 400std CPSI).

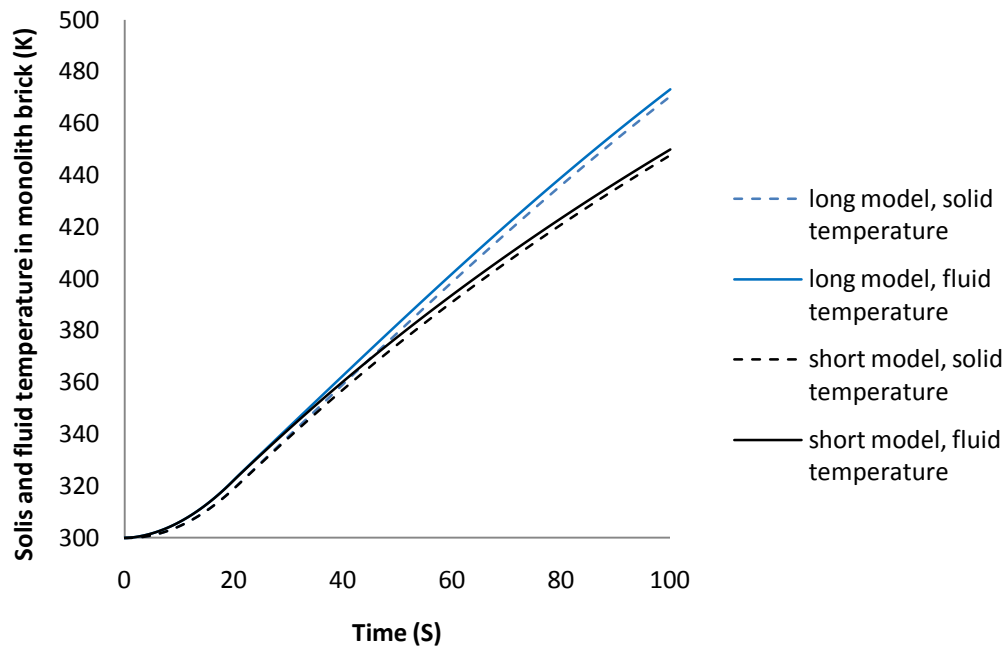


Figure 4.29-Average solid and fluid temperatures in the 400 std CPSI monolith brick with time for a feed with 0.02 Kg/s mass flow rate are shown. Long and short length models are compared.

### 4.3 Conversion profiles in the converter

In this section, CO and oxygen is reacting in the monolith brick. Involved parameters are discussed in detail in sections, 3.2 and 3.3. Fluid containing 1000 ppm CO and 10% oxygen with the rate of 0.02 Kg/s is introduced into the converter. This feed is also heated up at the inlet of the converter with the rate of 20 K/s from 300 K to 700 K in 20 seconds and remains constant at 700 K afterwards, during this time feed composition and mass flow rate remains constant. In the monolith brick, CO and O<sub>2</sub> react with the mechanism explained before. Light-off point and overall conversion of CO after 100 seconds of the converter operation is studied and the effect of different parameters on these two factors are investigated.

### 4.3.1 The effect of CPSI on conversion profile

In this section, middle size geometry is chosen as the basis and the effect of different CPSI configurations on the conversion profile of each converter is studied. In Figure 4.30, the results are shown. There is a considerable difference between 400 CPSI monolith and the other two monoliths in terms of conversion behavior. Light-off point ( the point with 50% conversion) of 400 CPSI monolith occurs at about 45 seconds after the operation, while this point for 900 CPSI and 400-thin CPSI monoliths occur much sooner, about 21 seconds after the operation. There are several parameters involved in this behavior of 400 CPSI monolith brick. As discussed in section 4.2.1, 400 CPSI monolith brick warms up late with respect to other monolith configurations. Lower velocity in the channels and higher thermal mass of this type of monolith are the main reasons in this regard. Considering first order reaction which occurs in the monolith brick and its Arrhenius term which is temperature dependant, temperature plays a very important role in conversion behavior of the converter. Another important factor is mass transfer resistance existed in the channels. Mass transfer coefficient,  $k_m$ , is one of the main factor that affect conversion profile of each monolith brick. This coefficient is inversely proportional to hydraulic diameter of the channel,  $D_H$ . Therefore, for 400 CPSI monolith brick this has the biggest channel diameter among other monoliths, this coefficient is the lowest and therefore much resistance in mass transfer from the fluid bulk to catalyst surface exist in this monolith. The combined effects of these parameters have lead to this considerable difference between light-off behavior of 400 CPSI monolith brick and the other two.

This fact has also shown in Table 3.4. Typical values for different parameters are calculated at 450 K. 900 CPSI monolith brick has the lowest mass transfer resistance, and therefore it has the highest reaction rate for that typical temperature. In Figure 4.27, we can see the same trend. Light-off points for 400-thin and 900 CPSI configurations are very close to each other, but due to higher

rate of reaction for 900 CPSI monolith brick, overall conversion of this monolith is about 8% higher than 400-thin CPSI.

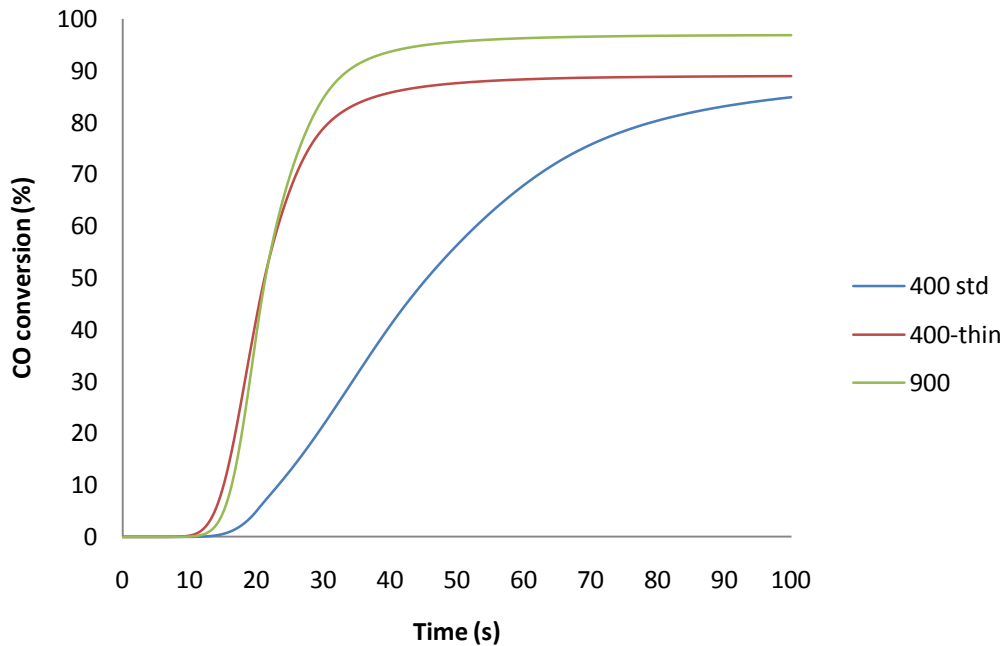


Figure 4.30-CO Conversion for different monolith CPSI configurations. Inlet mass flow rate is 0.02 Kg/s. Middle size converter is considered.

### 4.3.2 The effect of converter size on conversion profiles

400 CPSI monolith brick is the most widespread and popular monolith brick which is used in cars. So in this section, it was chosen as the basis and the effect of converter size on conversion profile of CO was investigated. The results are shown in Figure 4.28. As far as all parameters regarding monolith brick is the same for all simulation in this part, flow distribution and warm-up profile is playing the dominant role in order to understand the behavior of each converter conversion. As discussed before in section 4.2.2, average temperature of the monolith brick decreases when size of the reactor decreases. Therefore, average temperature of monolith brick in short size converter is the least among the others. This fact explains the least CO conversion in short size converter. As it is shown

in Figure 4.28 light-off point for long size converter is about 41 seconds, increasing to 55 seconds for the short size. Also after 100 seconds, long size converter shows a 15% higher conversion of CO with respect to the short one, making the short geometry as an ineffective model for the converter.

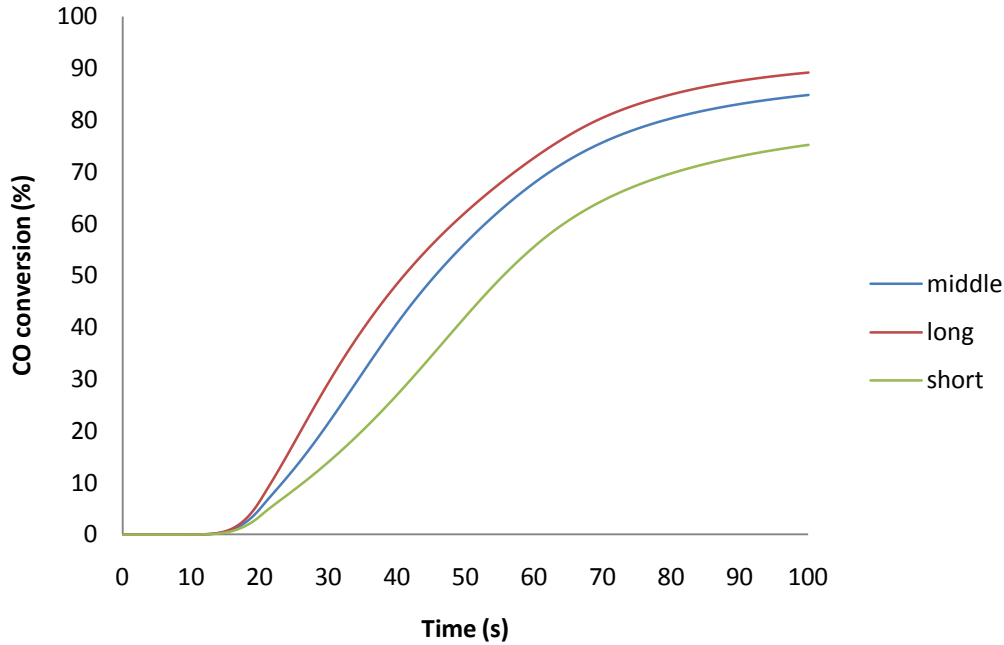


Figure 4.31- CO conversion for short, middle and long length converters. Inlet mass flow rate is 0.02 Kg/s and monolith brick is 400 CPSI std.

### 4.3.3 The effect of inlet cone on conversion profiles

In this part, middle size geometry is the basis and the effect of inlet cone size increasing on conversion behavior of three types of monolith is investigated. The results are shown in Figure 4.29. Based on the results, inlet cone size increasing do not change the overall order of CO conversion in terms of monolith brick type. Again, the best light-off and overall conversion result is for 900 CPSI monolith brick, and 400-thin and 400 CPSI types are in the next order. Also, for 400-thin and 400 CPSI monolith bricks, increasing the size of inlet cone have not much effect in light-off point and final conversion after 100 seconds. For the case of 900

CPSI, light-off point is reduced about 3 seconds but final conversion remains the same.

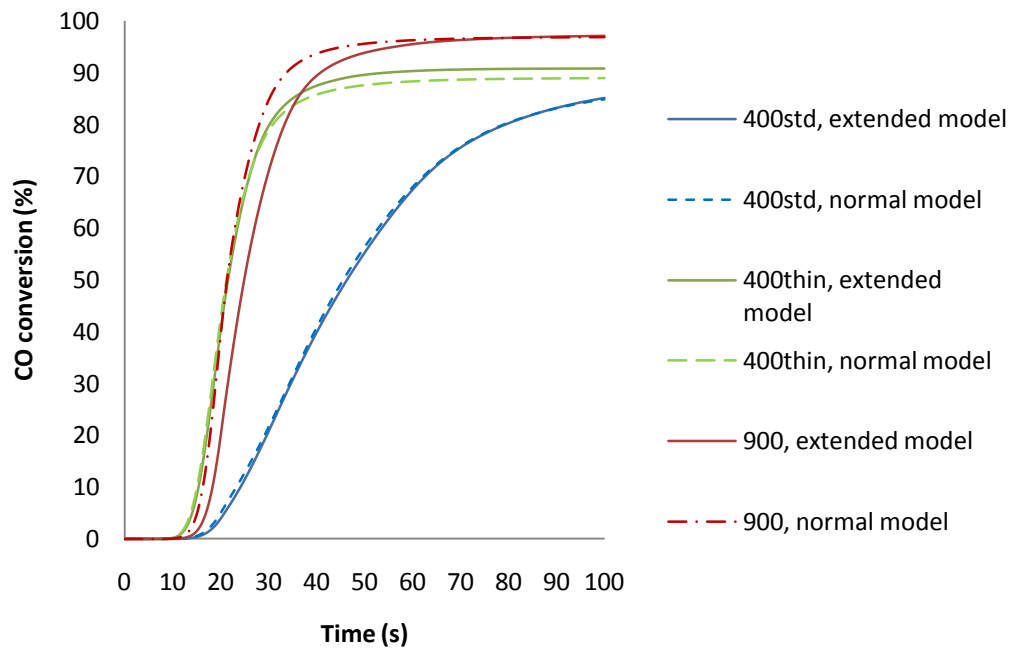


Figure 4.32-CO conversion for different monolith CPSI configurations. Middle length converter is the basis and inlet cone extended from 5 cm to 10 cm. Inlet mass flow rate is 0.02 Kg/s

# Chapter 5

## Conclusion and recommendations

In this work, a transient, two-dimensional continuous heterogeneous model has been developed and applied. The effect of different parameters, which are inlet mass flow rate, monolith brick CPSI configuration, size of the converter, and the effect of inlet cone on flow patterns, temperature profiles and light-off behavior of the converter, is discussed. A heterogeneous model was used to describe the monolith brick and a simple first order reaction was regarded for CO oxidation. The results presented in three sections.

### 5.1 Conclusions

In cold flow simulations, 400 CPSI with thin walls, showed the lowest pressure drop. Also, middle size geometry had the lowest eddies occurring in the converter.

In transient simulations, temperature profile and warm up behavior of the converter was discussed. In this part, 400 CPSI with thin walls warmed up faster than other CPSI configurations. Also, temperature difference between solid and fluid was negligible in this monolith brick. Due to weak circulation, short size converter warmed up later with respect to other converter sizes. Changing the size of the converter showed to have a negligible effect on the temperature difference between solid and fluid in the monolith brick.

In CO conversion section, the effect of CPSI configuration, converter size and inlet cone effect was presented. 900 CPSI monolith brick had the lowest time

needed for light-off. Also this configuration has the highest conversion after 100 seconds of converter operation; however none of the monolith bricks showed 100% conversion after 100 seconds. In this part, long converter showed the best light-off behavior with respect to other converter sizes and it had the highest CO conversion after 100 seconds. The effect of inlet cone increasing did not show much effect on the light-off and overall conversion behavior of the converter for 400 CPSI and 400 CPSI with thin walls; however it showed to have an effect on light-off behavior of 900 CPSI monolith brick.

## **5.2 Recommendations**

For further works, some suggestion can be made to gain a better understanding of both hydrodynamics and performance of the converter. These modifications will lead to more precise results and predict the actual behavior of the converter more accurately.

In this study, initial inlet temperature was 300 K. In cold regions, temperature can be much lower and as shown in this thesis, temperature is one of the main parameters in light-off behavior of a converter. The behavior of the converter in regions with colder inlet and ambient temperatures can be addressed. Also, inlet composition was considered constant in this study. In actual condition, composition of the inlet can vary based on the condition of the engine. Changing inlet velocity is another parameter that can be focused in future studies.

A 2D transient model was considered in this thesis. Computational power has increased considerably in recent years and this trend seems to be continuing in the future. So study on 3D models can be more feasible. 3D model can give better predictions and more accurate results.

In this study, a simple first order reaction was regarded for CO conversion. More realistic kinetic models can be used in future studies. Also, coupling methane oxidation kinetics with CO oxidation can be done for better predictions of actual

condition. Using look-up tables instead of rate equation is another issue that lowers the computation power and can be addressed in future studies.

# References

Chakravarthy, V.K., Conklin, J.C., Daw, C.S., D'Azvedo, E.F., "Multi-dimensional simulations of cold-start transient in a catalytic converter under steady inflow conditions", Applied Catalysis A: General 241, 289-306, 2003.

Chen. J., Yang, H., Wang, N., Ring, Z., Dabros, T., " Mathematical modeling of monolith catalysts and reactors for gas phase reactions", Applied catalysis A: General, 345,1-11, 2008.

Groppi, G., and Tronconi, E., "Simulation of Structured Catalytic Reactors With Enhanced Thermal Conductivity For Selective Oxidation", Catalysis Today, 69:63-73, 2001.

Gupta, N., and Balakotaiah, V., "Heat and Mass Transfer Coefficients in Catalytic Monoliths", Chem. Engg. Sci., 56 , 4771-4786 ,2001.

Government of Canada. [http://www.ec.gc.ca/pdb/ghg\\_home\\_e.cfm](http://www.ec.gc.ca/pdb/ghg_home_e.cfm), last visited July 2010.

Hayes, R.E., and Kolaczkowski, S.T., "Introduction to catalytic combustion", Gordon and Breach science publishers, 1997.

Hayes, R.E., Bertrand, F.H., Audet, C., and Kolaczkowski, S.T., "Catalytic Combustion Kinetics: Using a Direct Search Algorithm to Evaluate Kinetic Parameters from Light-off Curves", Can. J. Chem. Eng., Vol. 81, 1192-1199 ,2003.

Hayes, R.E., and Kolaczkowski, S.T., "Mass and Heat Transfer Effects in Catalytic Monolith Reactors", Chem. Eng. Sci., Vol. 49, 3587-3599 ,1994.

Hayes, R.E., Liu, B., and Votsmeier, M., "Calculating effectiveness factors in nonuniform washcoat shapes", Chem. Eng. Sci., Vol. 60, 2037, 2005.

Heck, R.H., Wei, J., and Katzer, J.R., "Mathematical Modelling of Monolithic Catalysts", AIChE Journal, 22, 477-484, 1976.

Hegedus, L.L., Oh, S.H., and Baron, K., "Multiple Steady State in an Isothermal Integral Reactor: The Catalytic Oxidation of Carbon Monoxide over Platinum-alumina", AIChE Journal, 23, 632-642, 1977.

Jeong, S., Kim, W., " A numerical approach to investigate transient thermal and conversion characteristics of automotive catalytic converter", International congress and exposition, Michigan, Feb 23-28, 1998.

Liu, B., Chekel, M.D., Hayes, R.E., Zheng, M., and Mirosh, E., "Transient simulation of a catalytic converter for a dual fuel engine" , Canadian Journal of Chemical Engineering, 78:557-568, 2000.

Liu, B., Hayes, R.E., Yi, Y., Mmbaga, J., Checkel, M D., and Zheng, M., "Three dimensional modeling of methane ignition in a reverse flow catalytic converter", Computers and Chemical Eng., 31, 292-306, 2007.

Martin, A. P., Will, N. S., Bordet, A., Cornet, P., Gondoin, C., Moutoun, X., "Effect of flow distribution on emissions performance of catalytic converters", International congress and exposition, Michigan, Feb 23-28, 1998.

Ramanathan, K., Balakotaiah, V., and West, D.H., "Geometry effects on ignition in catalytic monoliths", AIChE J., Vol. 50, 1493, 2004.

Ramanathan, K., Balakotaiah, V., and West, D.H., "Light-off Criterion and Transient Analysis of Catalytic Monoliths", Chem. Eng. Sci., Vol. 58, 1381-1405, 2003.

Ramanathan, K., Balakotaiah, V., and West, D.H., "Ignition Criterion for General Kinetics in a Catalytic Monolith", AIChE J., Vol. 52, No. 4, 1623-1629, 2006.

Shi-jin, S., Jian-xin, W., Ren-jun, Z., and Jun-rui, C., "Study on flow characteristics of automotive catalytic converters with various configurations", Society of automotive Eng. Inc., 01, 0208, 2000.

Tsinoglou, D.N., Koltsakis, G.C., Missirlis, D.K., Yakinthos, K.J., "Transient modelling of flow distribution in automotive catalytic converters", Applied mathematical modelling, 28 775-794, 2004.

Voltz, S. E., Morgan, C. R., Leiderman, D., and Jacob, S. M., "Kinetic study of carbon monoxide and propylene oxidation on platinum catalysts", Industrial engineering chemistry, production, research and development. **12**, 294-301, 1973.

Zygourakis, K., "Transient operation of monolith catalytic converters: A two-dimensional reactor model and the effects of radially nonuniform flow distributors", Chemical Engineering Science, 44(9):2075–2086, 1989.